1	Bridging the polarimetric structure and lightning activity of isolated
2	thunderstorm cells during the cloud life cycle
3	Chuanhong Zhao, ^{1,2} * Yijun Zhang, ^{1,3} * Huiyan Zhai, ² Zhe Li, ¹ Dong Zheng, ⁴ Xueyan Peng, ² Wen
4	Yao, ⁴ Sai Du, ⁵ Yuanmou Du, ⁶
5	Affiliations
6	¹ Department of Atmospheric and Oceanic Sciences & Institute of Atmospheric Sciences, Fudan
7	University, Shanghai, 200438, China.
8	² Plateau Atmosphere and Environment Key Laboratory of Sichuan Province, School of Atmospheric
9	Sciences, Chengdu University of Information Technology, Chengdu, 610225, China.
10	³ Shanghai Key Laboratory of Ocean-land-atmosphere Boundary Dynamics and Climate Change &
11	Shanghai Frontiers Science Center of Atmosphere-Ocean Interaction, Fudan University, Shanghai,
12	200438, China.
13	⁴ State Key Laboratory of Severe Weather, Chinese Academy of Meteorological Sciences &
14	Laboratory of Lightning Physics and Protection Engineering, Chinese Academy of Meteorological
15	Sciences, Beijing, 100081, China.
16	⁵ Guangdong Meteorological Service, Guangzhou, 510080, China.
17	⁶ Beijing Weather Modification Center, Beijing, 100089, China.
18	
19	
20	
21	
22	
23	Corresponding authors: Dr. Yijun Zhang & Dr. Chuanhong Zhao are the co-corresponding authors.
24	E-mail: zhangyijun@fudan.edu.cn; zch@cuit.edu.cn
25	
26	
27	
28	
20	

Abstract

30

31

32

33

34

35

36

37

38

39

40

41

42

43

44

45

46

47

48

49

50

51

52

53

54

55

Polarimetric structures detected by radar can characterize cloud microphysics and dynamics. Many studies have indicated that differential reflectivity (Z_{DR}) and specific differential phase (K_{DP}) columns, which serve as proxies for updraft strength, are related to lightning activity; moreover, the quantities of ice and supercooled liquid water strongly influence the occurrence of lightning flashes via noninductive charging. However, the sequence or interactions among these factors with dynamics and microphysics from the perspective of the cloud life cycle are uncertain. Here, we improve the '3D mapping columns' method to identify and quantify the Z_{DR}/K_{DP} columns, which is based on Cartesian grid datasets; this method is sensitive in the early phase of cloud formation. Our study bridges the polarimetric structure and lightning activity within fifteen isolated thunderstorms during the cloud life cycle. The results indicate that microphysical variations in supercooled liquid water and graupel yield better correlation coefficients for the lightning activity prediction at short warning times (e.g., 6 minutes) than dynamical variations in the Z_{DR} column volume do; however, the trend of the Z_{DR} column volume implies good performance at longer warning times (e.g., 12 minutes). The K_{DP} column is likely absent in the early phase of convection development; however, it will occur in the later stage with heavily cold cloud processes, replacing the Z_{DR} column to indicate updrafts within the reflectivity core when obvious graupels and hailstones occur. Our study improves the understanding of the polarimetric structure, which is related to dynamics and microphysics, and is also associated with lightning activity.

Short summary

Lightning activity is highly related to the signatures of polarimetric radar on the basis of cloud electrification physics. However, few studies have focused on bridging the polarimetric structure and lightning activity during the cloud life cycle. Here, we evaluated the sequence and interactions of polarimetric parameters for indicating lightning activity from the perspective of the cloud life cycle, and the cloud microphysics of the polarimetric structure were explored.

Keywords: thunderstorm; lightning activity; cloud microphysics; polarimetric radar

56

57

58

59

1.Introduction

Lightning is a traditional indication of severe weather (e.g., tornado, hail, microbursts, etc.).

Trends in lightning activity are useful for determining the severity of a thunderstorm (e.g., Gatlin

and Goodman, 2010; Goodman, et al., 2005; Williams, et al., 1999; Zhang et al., 2009). Lightning activity is the electrical response to dynamic conditions (updraft or turbulence) and cloud microphysics during storm evolution, which is supported by both theoretical and field observational studies of dynamics, microphysics and lightning activity (lightning initiation or total lightning flash rate) (e.g., Baker, et al., 1999; Baker, et al., 1995; Carey and Rutledge, 2000; Mitzeva and Saunders, 1990; Souza and Bruning, 2021; Williams, et al., 1989; Zhang et al., 2004a; Zhao, et al., 2021a). Notably, many studies have focused on the relationship between lightning activity and cloud updraft or microphysics (e.g., Carey and Rutledge, 1996, 2000; Deierling and Petersen, 2008; Lang and Rutledge, 2011; López and Aubagnac, 1997; Sharma, et al., 2024; Sharma, et al., 2021).

Polarimetric radar can provide observations to improve our understanding of the coupling between convective dynamics and storm microphysics (e.g., Sharma, et al., 2024). Lightning location technology can be used to monitor the occurrence of lightning flashes in real time (e.g., Rison, et al., 1999). In this way, radar and lightning observations can be used to link cloud updrafts and microphysics with lightning activity.

Carey and Rutledge (2000) utilized a C-band polarimetric radar to study the relationship between precipitation and lightning during tropical island convection events; their results indicated that lightning activity and the surface electric field are strongly correlated with the mixed-phase ice mass and rainfall properties during the mature phase of convection. Cloud-to-ground (CG) lightning was associated with the production and subsequent descent of graupel and frozen drops from the -10 to -20°C region; moreover, peaks in the CG lightning flash rate typically lagged behind peaks in the graupel mass aloft (Carey and Rutledge, 2000). This observational phenomenon reflects the noninductive charging between ice-phase hydrometeors, mainly graupel and ice crystals (e.g., Latham and Dye, 1989; Reynolds, et al., 1957; Saunders, 2008; Takahashi, 1978).

Before the formation of ice particles (e.g., graupel), the supercooled raindrops present in the mixed-phase zone throughout the developing and mature phases play crucial roles in storm kinematics, microphysics, and electrification. During freezing, supercooled raindrops likely provide (i) an instantaneous and abundant supply of millimetre-sized ice, (ii) a potential source of secondary ice particles, and (iii) an invigoration in the updraft due to the latent heat of freezing (Carey and Rutledge, 2000; Rosenfeld, et al., 2008; Zhao, et al., 2024; Zhao, et al., 2022). Moreover, millimetre-

sized ice and secondary ice particles contribute to cloud electrification (Bringi, et al., 1996; Sharma, et al., 2024). The intensity of convective updrafts through the modulation of microphysical factors, the collision efficiency of ice particles, and the electrification temperature influence the charge structure of storms (Liu, et al., 2024; Marshall, et al., 1995; Qie, et al., 2000; Yan et al., 1996a, b; Zhang, et al., 2004b), the flash size (Bruning and MacGorman, 2013; Zheng and Zhang, 2021), and the associated lightning flash rate (Deierling and Petersen, 2008; Deierling, et al., 2008; Fridlind, et al., 2019; Souza and Bruning, 2021; Zhao, et al., 2021a).

Moreover, supercooled raindrops produce a differential reflectivity (Z_{DR}) column, one of the most notable polarimetric radar signatures of convective storms. High Z_{DR} values (e.g., >1 dB) above the 0°C isotherm height (melting level) are associated with large supercooled raindrops and wet hail suspended in deep convective updrafts (e.g., Krause and Klaus, 2024; Kumjian, et al., 2014; Snyder, et al., 2015; Zhao, et al., 2020). Depending on the intensity of the updraft, the region of high Z_{DR} can extend several kilometres above the 0°C isotherm height. This narrow vertical extension of high Z_{DR} values above the environmental 0°C level associated with updrafts in strong convective storms is called the Z_{DR} column (Krause and Klaus, 2024; Kumjian, et al., 2014; Zhao, et al., 2020).

The Z_{DR} columns, due to the vertical size sorting of drops in warm-rain precipitation processes, encompass the signals of both microphysical features and updrafts; however, these signals are not present throughout the life cycle of strong convective storms, except in the early phase of cloud development. During the initial phase of a thunderstorm, the Z_{DR} column above the melting level indicates the presence of a low concentration of large raindrops (>2 mm); in addition, the Z_{DR} column expands downwards from above due to the collision and coalescence of drops and the accretion of droplets, resulting in the formation of larger raindrops (>4–5 mm) (Kumjian, et al., 2014). During the mature phase of a thunderstorm, the Z_{DR} column above the melting level may continue expanding upwards and outwards because stronger updrafts loft raindrops upwards into the mixed-phase layer, but smaller drops reach their nucleation temperature and begin to freeze while ascending to higher altitude. As these supercooled raindrops begin to freeze and mix with water-coated graupel and hail, the corresponding Z_{DR} values decrease, denoting top of the Z_{DR} column. As updrafts subsequently weaken and large ice particles (high-density graupel or hailstones) increase in abundance, the Z_{DR} column starts to collapse; however, lightning activity may exhibit

an inverse trend compared with that of the Z_{DR} column at this moment. For example, as shown by Sharma et al. (2024), after the first lightning jump, the subsequent lightning jumps are associated with a decreasing trend in the Z_{DR} column volume.

On the other hand, in the specific differential phase (K_{DP}) column, high values (>0.75°/km, the value reported by Loney et al. (2002)) above the melting level occur and are strongly associated with a high concentration of water-coated ice (e.g., water-coated graupel and hail with a non-spherical shape) and raindrops (1–2 mm) that shed from hailstones growing in a wet regime (Bringi, et al., 1996; Hubbert, et al., 1998; Loney, et al., 2002). Thus, the formation of a K_{DP} column is tied to cold cloud microphysics, which usually lag behind the appearance of the Z_{DR} column.

van Lier-Walqui et al. (2016) attempted to constrain cloud-resolving models on the basis of ground-based remote sensing observations, namely, polarimetric radar data. In their study, the K_{DP} column (specifically, the column volume) was strongly related to the updraft mass flux, lightning activity, and rainfall intensity in four deep convection events observed during the Midlatitude Continental Convective Clouds Experiment. Recently, Sharma et al. (2024) utilized polarimetric radar observations of three severe storms during the VORTEX-Southeast field campaign to quantify the correlation between the volumes of Z_{DR} and K_{DP} columns (representative of mixed-phase microphysics as well as updraft intensity and size) and total lightning flash rates. They indicated that the volume of the K_{DP} columns exhibited high co-variability with the total flash rate in three such cases (a tornadic supercell embedded in a stratiform precipitation system, a non-tornadic supercell, and a supercell embedded within a quasilinear convective system).

Sharma et al. (2024) conducted a study on the basis of hypotheses, namely, that the deeper and wider the Z_{DR} and K_{DP} columns were in cases with robust and wide updrafts (e.g., Homeyer and Kumjian, 2015; Snyder, et al., 2017), the more an increase in the volumes of the Z_{DR} and K_{DP} columns would correspond to an increase the mixed-phase ice mass flux, resulting in an increase in the total flash rate; the correlation coefficient ($-0.47 \sim 0.37$ for the Z_{DR} column; 0.54 \sim 0.74 for the K_{DP} column) between Z_{DR} or K_{DP} columns and lightning activity was not as high as the microphysical parameters explored in previous studies (e.g., Carey and Rutledge, 2000). Moreover, the results seem to be inconsistent with those of Sharma et al. (2021), who reported that the variability in flash rates is best explained by fluctuations in the Z_{DR} column volume, with a high

correlation coefficient value (0.72). One possible explanation is that the effect of the time lag may decrease this correlation coefficient. As reported by Carey and Rutledge (2000), they obtained a very high one-lag (7 minutes) correlation coefficient (ρ = 0.9) between the graupel mass within the mixed-phase zone and the CG lightning flash rate, suggesting that the directly related microphysics with noninductive charging have a greater correlation coefficient with lightning activity. Another possible way is that the interactions of the Z_{DR}/K_{DP} column with dynamics and microphysics are uncertain, which affects the results under the current hypotheses. This is also emphasized in Sharma et al. (2021) and raised as a retained question in the appendix. Thus, further exploration is needed.

In summary, dynamical and microphysical characteristics derived from polarimetric radar can provide forecasting information about lightning activity on the basis of noninductive charging: i) the precipitation-sized (e.g., graupel) ice mass within the mixed-phase zone; ii) the content of supercooled raindrops; and iii) the quantified Z_{DR} and K_{DP} columns (e.g., the column volume or height). Our goal in this study is to link these polarimetric radar variables for forecasting lightning activity within isolated thunderstorm cells during the cloud life cycle over South China, and determine how the cloud microphysics and dynamics related to these polarimetric radar variables should be assessed. Notably, the close relationship between these polarimetric radar variables and lightning activity has been noted in many studies (e.g., Carey and Rutledge, 2000; Hayashi et al., 2021; Sharma et al., 2024; Sharma, et al., 2021; Snyder, et al., 2015; van Lier-Walqui, et al., 2016; Woodard et al., 2012); thus, we believe that this study is sufficient for connecting these polarimetric radar variables and lightning activity via the anatomy of an isolated thunderstorm cell during the cloud life cycle and the statistical results of fifteen isolated thunderstorm cells.

This paper is organized as follows. In Section 2, an overview of the radar and lightning data is given, and the analysis methods and the approach for quantifying the Z_{DR}/K_{DP} columns are described. Section 3 presents the results of Z_{DR}/K_{DP} column quantification and the related characteristics of the polarimetric structure and microphysics with the Z_{DR}/K_{DP} column. The vertical structures of polarimetric radar variables and microphysics are explored in combination with 3D lightning location data. The relationship between lightning activity and these polarimetric characteristics in cases and statistics is presented. Finally, we summarize the results in Section 4.

2.Data and methodology

2.1. Radar and lightning observations

This study included 15 isolated thunderstorm cells that produced lightning, which was observed via an S-band dual-polarization radar deployed in Guangzhou city (GZ radar) and a low-frequency E-field detection array (LFEDA) (Table 1). The average 6-hourly convective available potential energy (CAPE) of these thunderstorms was obtained from ERA-Interim reanalysis data, as in Zhao et al. (2022). The detailed examination of lightning activity with related dynamics and microphysics in case #1 was conducted first, and then the statistical results of all cases were given. On 20 June 2016, one isolated thunderstorm cell was observed by the GZ radar(Figure 1). The composite reflectivity data revealed that this thunderstorm (the boundary was determined via manual inspection; the black lines in Figure 1) was nearly stationary and that the cloud life cycle lasted approximately two hours. Lightning activity occurred when values of composite reflectivity >35 dBZ were present; this phenomenon seemingly supported the results of Hayashi et al. (2021), highlighting the importance of graupel in cloud electrification.

Table 1. The information of cases

Cases number	Time information [CST]	CAPE [J kg ⁻¹]
#1	17:18 to 19:00, 20 June 2016	1277
#2	12:12 to 13:18, 26 June 2016	1225
#3	15:36 to 16:36, 3 July 2016	961
#4	16:06 to 17:06, 5 July 2016	412
#5	11:00 to 12:12, 6 July 2016	1202
#6	16:18 to 17:06, 6 July 2016	1202
#7	15:00 to 16:06, 16 July 2016	1425
#8	13:24 to 14:12, 27 July 2016	1203
#9	14:36 to 15:18, 27 July 2016	1376
#10	14:54 to 15:18, 27 July 2016	1286
#11	13:24 to 15:00, 29 May 2016	1339
#12	09:18 to 10:48, 18 June 2016	1437
#13	12:18 to 13:00, 18 June 2016	1375
#14	15:48 to 16:36, 18 June 2016	1475
#15	13:06 to 14:12, 7 July 2016	2537

The beam width of the GZ radar is $\leq 1^{\circ}$, and the azimuth and range resolutions are 1° and 250 m, respectively. A full radar volume scan lasted 6 minutes at nine elevation angles. The GZ radar data were processed via the Python ARM Radar Toolkit (Py-ART), including quality control (Helmus and Collis, 2016; Li, et al., 2023; Li, et al., 2024). The Z_{DR} offset of the raw data was corrected via drizzle, and the calibration accuracy was expected to be 0.1–0.2 dB (Bringi and Chandrasekar, 2001). We utilized two methods to smooth the differential phase Φ_{DP} , namely,

"lightly filtering" (2-km) and "heavily filtering" (6-km), as in Park et al. (2009). Two estimates of K_{DP} were subsequently obtained from a slope of a least squares fit of the filtered Φ_{DP} ; a lightly filtered K_{DP} was subsequently used in the case of horizontal reflectivity > 40 dBZ, and a heavily filtered K_{DP} was selected otherwise (Ryzhkov and Zrnić, 1996). The radar data were gridded via Py-ART gridding routines on a Cartesian grid with a 0.25-km horizontal resolution and a 500-m vertical resolution ("Barnes2" method).

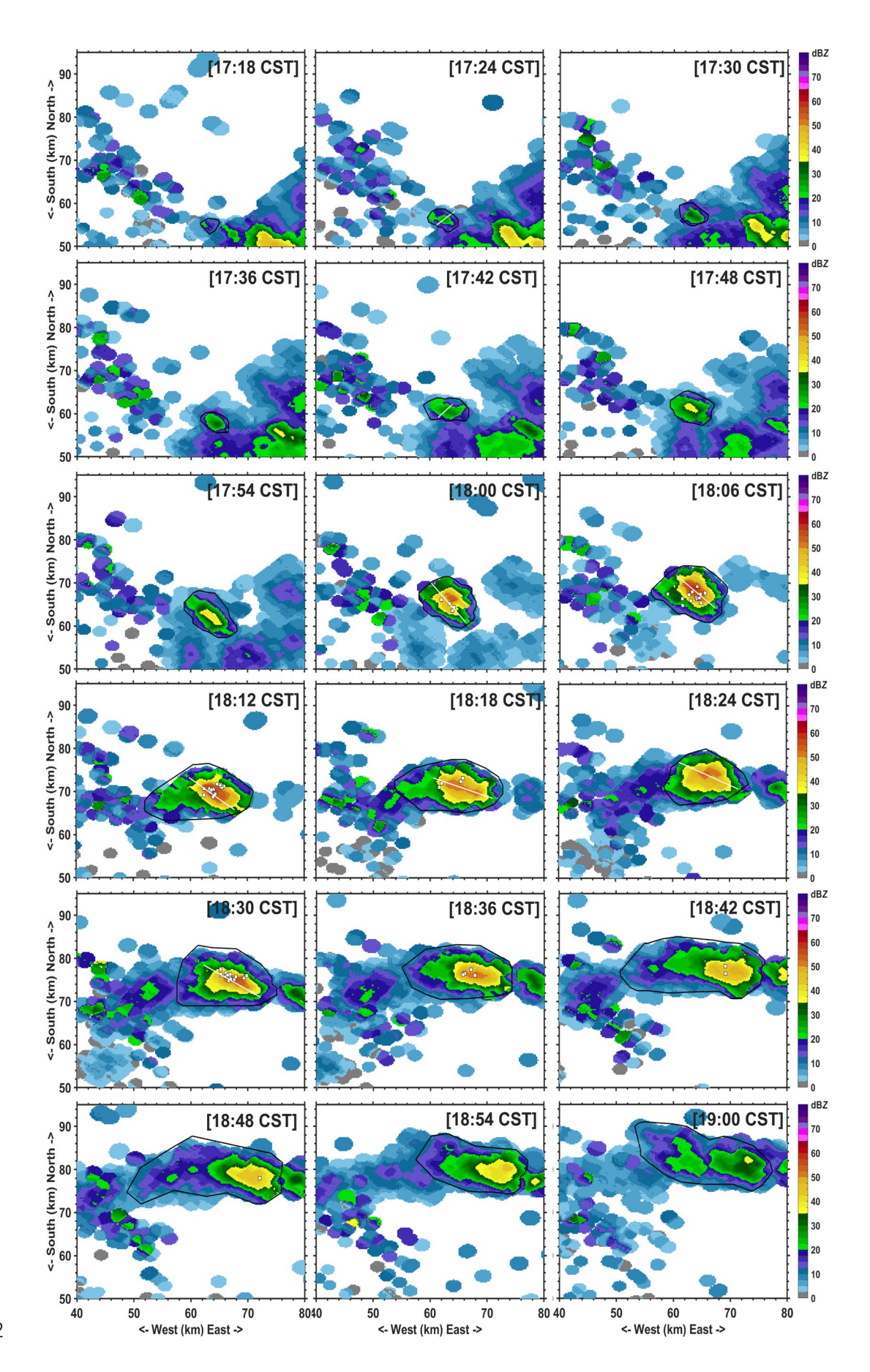


Figure 1. The composite reflectivity of the isolated thunderstorm cell on 20 June 2016 (case #1), which initiated at 17:18 and ended at 19:00 (China Standard Time, CST). The black lines indicate the boundary of this thunderstorm. The white squares (intracloud flashes) and triangles (CG flashes) indicate the lightning flashes, and the location of once lightning flash is represented by the location of the first discharge pulse event. The positions for the plotted cross section are shown as white lines over the composite reflectivity data.

The lightning flashes within this thundercloud were detected via LFEDA, which is a 3-D mapping detection system for intracloud and CG lightning, with 10 sensors. Previous studies (Fan, et al., 2018; Shi, et al., 2017) utilized information from triggered lightning flashes to evaluate LFEDA detection results; the results show the detection efficiency of the LFEDA can reach 100%, and the mean location error is 102 m. Discharge pulse events were grouped into a lightning flash via the same method as described by Liu et al. (2020). A potential discharge pulse event of one lightning flash should occur within 0.4 s of the previous discharge pulse event and within 0.6 s and 4 km of any other discharge pulse event of this lightning flash. If any source within one lightning flash is below the 2-km height, this lightning flash is regarded as one cloud-to-ground flash, as suggested by Zhao et al. (2021a).

The lightning flashes were assigned to the isolated thunderstorm on the basis of the boundary of the thunderstorm, as well as a constraint every 6 minutes (according to the duration of a full radar volume scan). The life cycle of this isolated thunderstorm initiated from the first radar echo (i.e., the presence of a maximum horizontal reflectivity $(Z_H) \ge 5$ dBZ in a full radar volume scan within this cloud was first detected by the GZ radar, as suggested by Zhao et al. (2021a, 2022, 2024)) and ended when the maximum Z_H started to decrease and the Z_H reached ≤ 40 dBZ. The distributions of these detection systems, including radar and lightning location system, were illustrated by in Zhao et al. (2024).

2.2. Cloud microphysical parameter retrieval methods

To estimate the precipitation-sized ice mass (e.g., graupel, hail, and frozen drops) and the content of supercooled raindrops within the mixed-phase zone, an approach on the basis of difference reflectivity (Z_{DP} , dB) is applied (Carey and Rutledge, 2000; Straka et al., 2000).

230
$$Z_h = (4\lambda^4/\pi^4|K_w|^2)\langle |S_{hh}|^2 \rangle$$
 (1)

231
$$Z_{\nu} = (4\lambda^4/\pi^4|K_{\nu}|^2)\langle|S_{\nu\nu}|^2\rangle$$
 (2)

$$Z_{\rm DP} = 10 \log_{10}(Z_h - Z_v), \text{ for } Z_h > Z_v$$
 (3)

 S_{ij} refers to an element of the backscattering matrix of a hydrometeor (Zrnić, 1991). The first subscript i indicates the polarization of the backscattered field (h is horizontal, v is vertical), and the second subscript j indicates the polarization of the incident field. $K_w=(\epsilon_w-1)/(\epsilon_w+2)$ is the factor associated with the dielectric constant of water, and ϵ_w is the dielectric constant. λ is the radar wavelength. The brackets indicate expectations expressed in terms of the distribution of mean hydrometeor properties such as shape, size, fall orientation, particle density, canting angle, dielectric constant, and others.

Pruppacher and Klett (1997) assumed that precipitation-sized ice particles were more spherically symmetrical or tumble. The low dielectric constant and significant canting behaviour of ice particles likely result in a near-zero Z_{DR} (e.g., Seliga and Bringi, 1976). Therefore, the horizontal reflectivity and vertical reflectivity are equal for ice particles, as "effective spheres", and Z_{DP} is solely influenced by raindrops. If the relationship between horizontal reflectivity and Z_{DP} (raindrops) is known, the horizontal reflectivity of raindrops can be derived. The relationship between the horizontal reflectivity of raindrops and Z_{DP} (raindrops) is derived from 2-year disdrometer data in Guangdong Province (Li et al., 2019), which is suitable for the current radar used in this study:

$$Z_{H}^{rain} = 0.0044 Z_{DP}^{2} + 0.58054 Z_{DP} + 16.591$$
 (4)

Then, the ice echo intensity $Z_{\rm H}^{\rm ice}$ can be expressed as $Z_{\rm H}-Z_{\rm H}^{\rm rain}$. The standard error for the relationship between horizontal reflectivity and $Z_{\rm DP}$ is consistently approximately 1 dB (Carey and Rutledge, 2000). If $Z_{\rm H}-Z_{\rm H}^{\rm rain}<1$ dB, which is below the melting layer, $Z_h^{\rm ice}=0$ mm⁶m⁻³, $Z_{\rm H}^{\rm rain}=10\log_{10}(Z_h^{\rm rain})$, and $Z_h^{\rm rain}=Z_h$. In contrast, above the melting layer, if $Z_{\rm H}-Z_{\rm H}^{\rm ice}<1$ dB, then $Z_h^{\rm rain}=0$ mm⁶m⁻³, and $Z_h^{\rm ice}=Z_h$ (Carey and Rutledge, 2000). The estimates of rain mass ($M_{\rm w}$, g m⁻³) and ice mass ($M_{\rm ice}$, g m⁻³) are derived via the following reflectivity–mass relationships (Chang et al., 2015; Zhao et al., 2022):

256
$$M_w = 3.44 \times 10^{-3} \left(Z_h^{rain} \right)^{4/7} \tag{5}$$

$$M_i = 1000\pi \rho_i N_0^{3/7} \left(\frac{5.28 \times 10^{-18} Z_h^{ice}}{720} \right)^{4/7}$$
 (6)

where ρ_i indicates the ice density (kg m⁻³), N_0 =4×10⁶ m⁻⁴. The estimated ice mass from the horizontal reflectivity of ice particles is proportional to the actual ice mass and depends on the

variability in the intercept parameter of an assumed inverse exponential distribution for ice and the ice density; thus, the trends of the estimated ice mass are deemed sufficient to investigate lightning activity. Importantly, the Z_{DP} can differentiate between ice and rain only if the Z_H is sufficiently large (i.e., diameter ≥ 1 mm); under such conditions, the raindrop is characterized by significant oblateness (Carey and Rutledge, 2000; Green, 1975).

The estimated ice masses are assigned to graupel masses on the basis of scattering properties, namely, where the Z_H values exceed 35 dBZ (Carey and Rutledge, 2000; Kumjian, 2013a, b; Zhao, et al., 2021b). The threshold value is usually applied to identify graupel in hydrometeor identification method (Park et al., 2009). The rain water content above the melting level (0°C isotherm height; sounding data from the Qingyuan meteorological observatory are used to obtain the environmental temperature) is defined as the supercooled raindrop mass.

 Z_{DR} columns are associated with low concentration of large raindrops (>2 mm); thus, the median volume diameter D_0 of raindrops is retrieved via the method described by Hu and Ryzhkov (2022) to provide supporting evidence for identifying Z_{DR} columns. Notably, D_0 is not used to identify Z_{DR} columns directly but rather to ensure the threshold value of Z_{DR} , which is utilized to identify Z_{DR} columns directly. The fractional standard deviation of the D_0 estimation is approximately 10% (Hu and Ryzhkov, 2022).

To further explore the characteristics of the microphysics related to the Z_{DR}/K_{DP} column and lightning within these thunderstorms, hydrometeor identification method involving the fuzzy-logic algorithm (as in Zhao et al., 2021b) and the microphysical fingerprint (following Kumjian et al., 2022) are conducted. Identifying polarimetric radar "fingerprints" of ongoing microphysical processes was introduced by Kumjian (2012); these fingerprints are defined as vertical changes in two (e.g., Z_H , Z_{DR}) or more of the dual-polarization radar variables (Kumjian et al., 2022).

As suggested by Kumjian et al. (2022), the co-polar correlation coefficient (CC) is neglected in most of the fingerprints discussed but it is important to indicate the melting process; thus, we added the changes in the CC towards the ground to identify the melting process. The changes in the polarimetric radar variables towards the ground for riming and aggregation are the same (Kumjian et al., 2022); however, the riming process is valuable for studying lightning activity. Thus, we followed the method for identifying the aggregation and graupel particles in Park et al. (2009),

namely, we utilized the discriminated convective and stratiform echoes to determine where riming or aggregation processes occur. If the echo is classified as convective, then the aggregation process is not allowed within a whole vertical column; conversely, the riming process is excluded in the stratiform case.

In addition, the 0°C isotherm height is used to discriminate warm-rain processes and mixed-phase processes; notably, this rule introduces potential errors when it is used where the Z_{DR}/K_{DP} column is used. Specifically, the polarimetric characteristics of collision-coalescence and size sorting (or evaporation) processes above the 0°C isotherm height are regarded as vapour deposition and refreezing processes, respectively. In this study, we utilize the identified and quantified Z_{DR}/K_{DP} columns to correct this possible error. A summary of the changes in the polarimetric radar variables towards the ground and additional conditions for different microphysical processes is displayed in Table 2. To characterize the microphysical fingerprints in this study, the changes in the polarimetric radar variables towards the ground are computed between two adjacent grids in the vertical direction (for example, ΔZ_H (x, y, z₁) = Z_H (x, y, z₂) – Z_H (x, y, z₁), x, y, and z are the three dimensions in the Cartesian coordinate system; z₁ is 500 m in height, and z₂ is 1000 m in height). The minimum thresholds of $\Delta Z_H > 0.002$ dB/km and $\Delta Z_{DR} > 0.0001$ dB/km are applied to avoid false classifications based on noise present in the data, as in Kumjian et al. (2022).

Table 2. Changes in the polarimetric radar variables towards the ground for different microphysical processes. An increase in that radar variable between the top and bottom of the profile is indicated by a positive sign +, whereas a decrease is indicated by a negative sign.

Microphysical processes	$\Delta Z_{\rm H}$	ΔZ_{DR}	ΔCC	Convective/Stratiform area	Z _{DR} /K _{DP} column
Collision-Coalescence	+	+	/	/	$\sqrt{}$
Breakup	-	_	/	/	/
Size Sorting/Evaporation	_	+	/	/	$\sqrt{}$
Vapour Deposition	+	+	/	/	×
Aggregation	+	_	/	Stratiform area	/
Riming	+	_	/	Convective area	/
Sublimation (with	-	_	/	/	/
fragmentation)/Refreezing					
Refreezing	_	+	/	/	×
Melting	+	+	_	/	/

2.3. Previous automatic identification and quantification methods for Z_{DR}/K_{DP} columns

Currently, a few methods are available to automatically identify and quantify Z_{DR}/K_{DP} columns (e.g., Woodard et al., 2012; Krause and Klaus, 2024; Sharma, et al., 2024; Snyder, et al., 2015; van

Lier-Walqui, et al., 2016). These methods are constructed on the basis of the morphology of the Z_{DR}/K_{DP} columns and/or the high values (e.g., $Z_{DR} > 1$ dB; $K_{DP} > 1^{\circ}/km$) above the melting level.

In the stage of cloud formation, high Z_{DR} values above the melting level are simply used to identify Z_{DR} columns; however, these high values are not always associated with the Z_{DR} columns. Notably, three-body scatter signatures (Zrnić, 1987), depolarization streaks associated with the canting behaviour of ice in regions of strong electrification (Kumjian, 2013c), and oblate ice particles can lead to enhanced positive Z_{DR} values (Kumjian, 2013a). Thus, additional requirements were imposed to avoid identification errors, e.g., the reflectivity threshold value ($Z_H \ge 40 \text{ dBZ}$) (Woodard et al., 2012) and the height should be below the homogeneous melting level, and the maximum height of the Z_{DR} column should be associated with the height at which Z_{DR} displays a negative vertical gradient (van Lier-Walqui, et al., 2016).

Recently, Krause and Klaus (2024) utilized the hotspot technique to identify the base of the Z_{DR} column on the basis of constant altitude plan projection indicators (CAPPIs). Although their results indicated an improvement in the plan region identified on the basis of the Z_{DR} column approach over the results of two different existing algorithms (Thunderstorm Risk Estimation from Nowcasting Development via Size Sorting algorithm and the algorithm introduced by Snyder et al. (2015)), the depth and volume information for Z_{DR} columns was lost, which was not beneficial for forecasting lightning activity. In addition, the reflectivity threshold value ($Z_{H} > 25 \text{ dBZ}$) was required in this algorithm. Sharma et al. (2024) used an algorithm in the "scikit-image" Python package to identify Z_{DR}/K_{DP} columns from Cartesian grid data via threshold values ($Z_{DR} \ge 1 \text{ dB}$; $K_{DP} \ge 1^{\circ}/\text{km}$); they restricted the Z_{H} values to exceed 20 dBZ, and any instances of obvious data contamination or unrealistic values during the gridding process were manually removed prior to analysis. They focused on three supercells during lightning activity, and violent convection in such case will ignore the formation of Z_{DR}/K_{DP} columns at weak echo intensities, i.e., in the initiation stage of convective clouds.

2.4. Automatic 3D mapping of Z_{DR}/K_{DP} columns during the life cycle of an isolated cell storm

Our objective in this study is to explore the performance of microphysics retrieved via radar for forecasting lightning activity within isolated thunderstorm cells during the cloud life cycle. As depicted in Figure 1, our radar observations indicate that before the initiation of lightning, the echo intensity is weak during the early stage of a cloud. Moreover, we seek to determine whether Z_{DR} columns form in the early stages of cloud formation. In addition, K_{DP} columns are representative of small drops with high concentration shed from large ice particles (e.g., hailstones) growing in a wet regime (Hubbert, et al., 1998; Loney, et al., 2002).

Figure 2 shows the first appearance of the Z_{DR} column at 17:24 (China Standard Time, CST), which is ~36 minutes earlier than the first lightning occurrence and only lags behind the first radar echo by 6 minutes. The high values of Z_{DR} extend to the mixed-phase region from the cloud bottom, and the height of the Z_{DR} column is approximately 1 km (Figure 2c). The corresponding Z_H values are smaller than 30 dBZ, but with the values of the co-polar correlation coefficient (CC) are relatively high (Figure 2a, d). These characteristics indicate the presence of large raindrops with low concentrations; the low K_{DP} values and large size of raindrops (exceeding 2 mm) support that (Figure 2e, f). We illustrate the microphysical structure corresponding to high Z_{DR} values in Figure 2b. The threshold value for identifying the Z_{DR} column in this study is 1.5 dB, considering that the size of raindrops should exceed 2 mm within the Z_{DR} column during the initial phase of a storm (e.g., Kumjian, et al., 2014). In addition, the K_{DP} column is absent in the initial phase of this storm, not appearing until 18:30 CST.

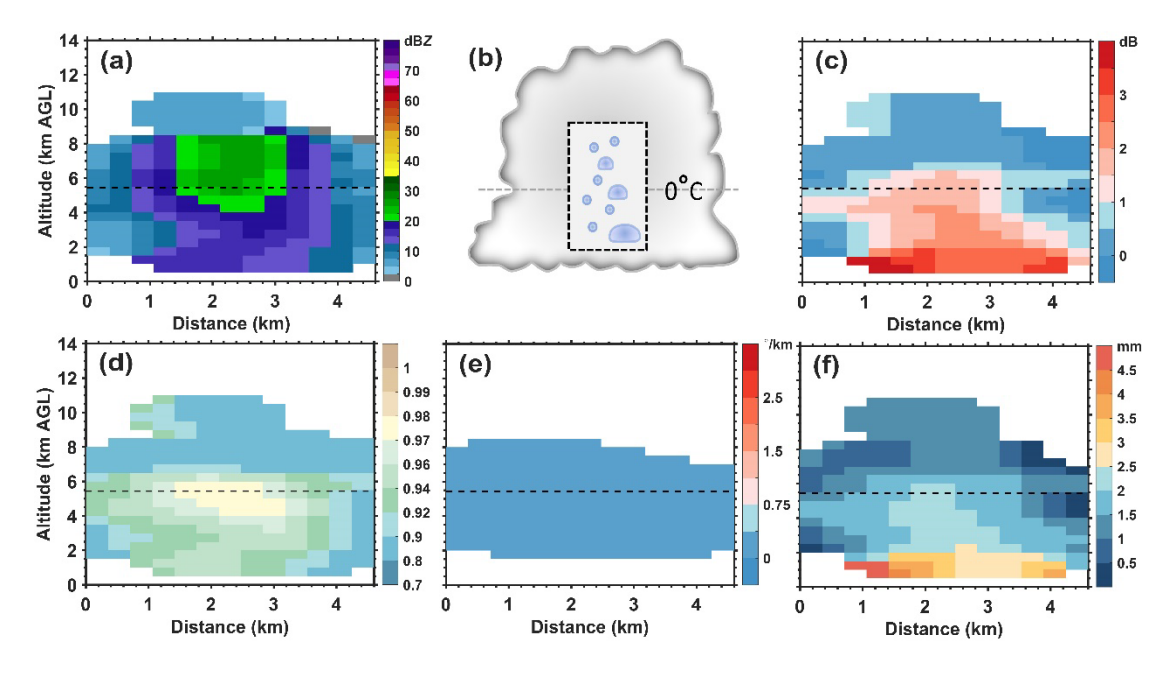


Figure 2. Cross section from the Cartesian grid of the studied isolated thunderstorm at 17:24 CST. (a) Z_{H} . (b) Conceptual model of the microphysical structure within high Z_{DR} values. (c) Z_{DR} , (d) CC, (e) K_{DP} . (f) Median

volume diameter D_0 of raindrops. The black dashed line indicates the 0°C isotherm height. AGL (above ground level).

In this study, we improved a method that only depends on the Z_{DR} parameter for identifying and easily quantifying the Z_{DR} column (e.g., height and volume) during the whole life cycle of a storm, specifically, including the initial phase of a convective cloud; the morphology of the Z_{DR} column resulting from size sorting and the high Z_{DR} values (≥ 1.5 dB) in Cartesian grid data are combined as the basis of this method. A flow chart of this method is depicted in Figure 3.

First, we establish logic matrices with the same specifications as the Z_{DR} matrices and identify the layer that corresponds to the 0°C isotherm height (with sounding data used to determine the environmental temperature). Second, from the 1-km height below the melting level to the mixed-phase region, if $Z_{DR} \ge 1.5$ dB, the corresponding logic values in the logic matrix are equal to 1. Notably, we utilize the lower portion of the logic matrix to upwards restrict the possible errors associated with including locations outside the successive column of high Z_{DR} values (≥ 1.5 dB). This restriction condition is based on the column morphology (columnar shape), which results from drop size sorting. Specifically, the region of the Z_{DR} column contracts upwards from the 0°C isotherm height below the mixed-phase region (e.g., as shown in Amiot et al. (2019), Hubbert et al. (2018), Kumjian et al. (2014), Snyder et al. (2015) and Tuttle et al. (1989)). In the Cartesian grid data, this phenomenon is particularly obvious (Figure 2c).

Third, the size distribution of raindrops within the Z_{DR} column is determined by size sorting; thus, we utilize the negative vertical gradient of Z_{DR} on the basis of every grid between two adjacent layers from the 0° C isotherm height to the uppermost limit height to further ensure that the grids are associated with the Z_{DR} column. Finally, a 3D mapping of the Z_{DR} column is constructed. We can use the grid information to compute the height and volume of the Z_{DR} column. Although the formation mechanism of the K_{DP} column is different from that of the Z_{DR} column, the morphology of the K_{DP} column is highly consistent with that of the Z_{DR} column; thus, this method can be applied to map the K_{DP} column with a 3D grid based on the threshold value for identifying the K_{DP} column (e.g., $\geq 1^{\circ}$ /km).

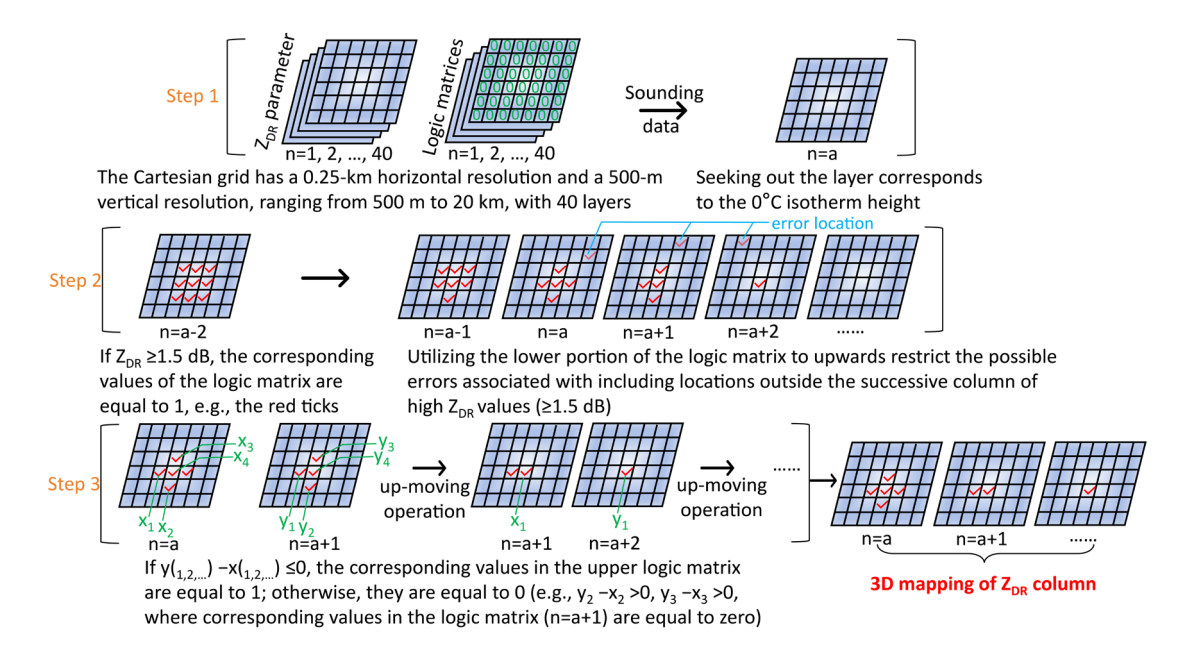


Figure 3. Flow chart of 3D mapping of a Z_{DR} column.

3. Results

3.1. Assessment of Z_{DR}/K_{DP} columns identified via the "3D mapping columns" method

Snapshots of the identified Z_{DR} columns via the "3D mapping columns" method at four moments (the K_{DP} column only existed at one moment during the life cycle of this thunderstorm) are shown in Figure 4. The identified regions of the Z_{DR}/K_{DP} columns are represented by white dots. We verify that the "3D mapping columns" method performs well in identifying the Z_{DR}/K_{DP} columns via manual inspection.

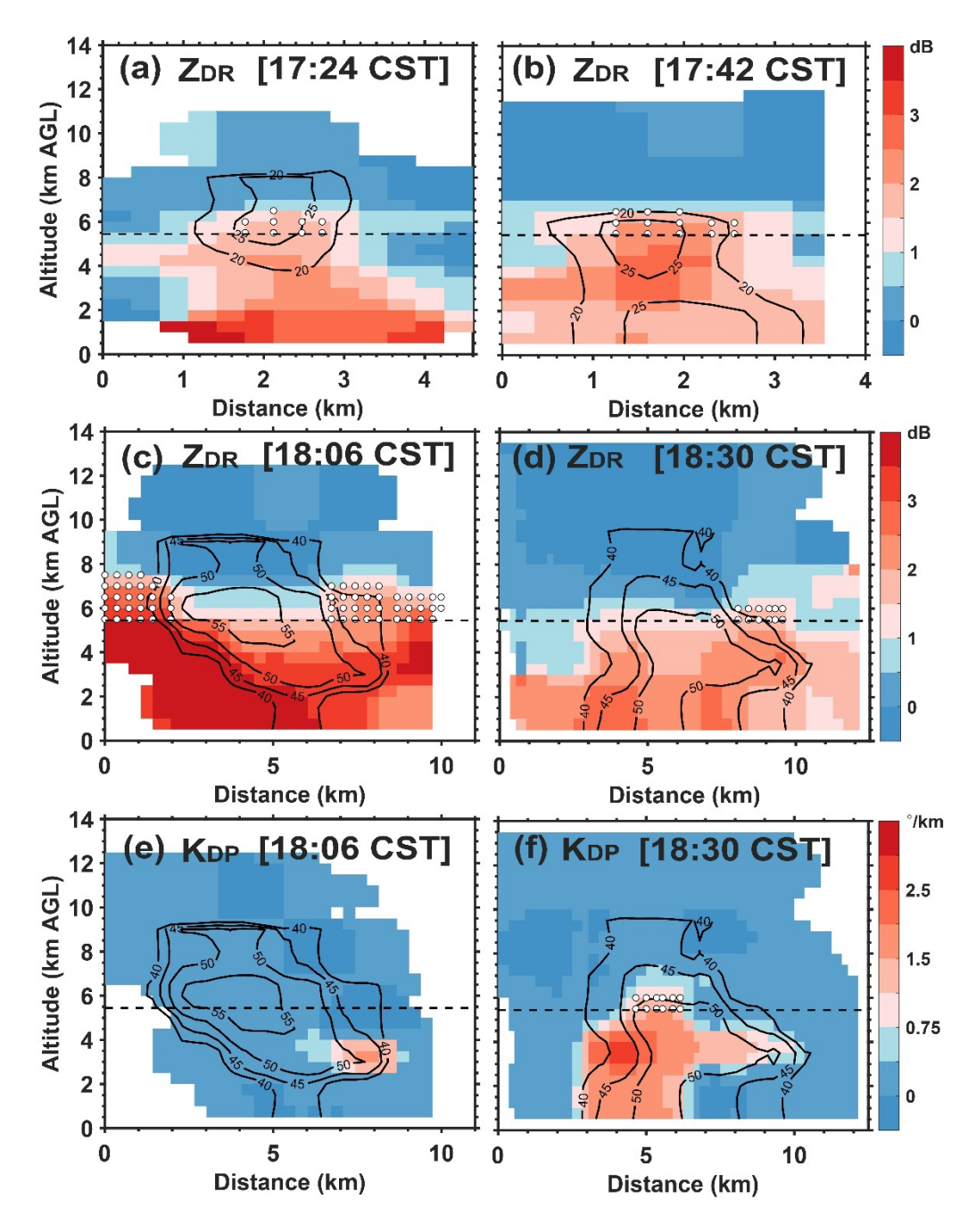


Figure 4. Cross sections from the Cartesian grid of the studied isolated thunderstorm at (a) 17:24 CST, Z_{DR}; (b) 17:42 CST, Z_{DR}; (c) 18:06 CST, Z_{DR}; (d) 18:30 CST, Z_{DR}; (e) 18:06 CST, K_{DP}; and (f) 18:30 CST, K_{DP}. The black

dashed line indicates the 0°C isotherm height. The white dots indicate the areas of the identified Z_{DR}/K_{DP} columns.

The black contours with values indicate the reflectivity structure. AGL (above ground level).

The first Z_{DR} column in this isolated thunderstorm occurred at 17:24 CST (Figure 4a, Figure 5a). The second Z_{DR} column subsequently occurred at 17:42 CST after 18 minutes (Figure 4b, Figure 5a). At 18:06 CST, the lightning activity reached the first peak (Figure 6; to compare the radar and lightning data, the lightning flash frequency was counted every 6 minutes), and the Z_{DR} column was

the largest (in volume) at this time (Figure 5a). However, the overlap region between the Z_{DR} column and reflectivity core at 17:24 and 17:42 CST disappeared at 18:06 CST (Figure 4c); i.e., the Z_{DR} column within the reflectivity core began to collapse because of the falling of large-sized (represented by Z_{H} values exceeding 40 dBZ) ice particles.

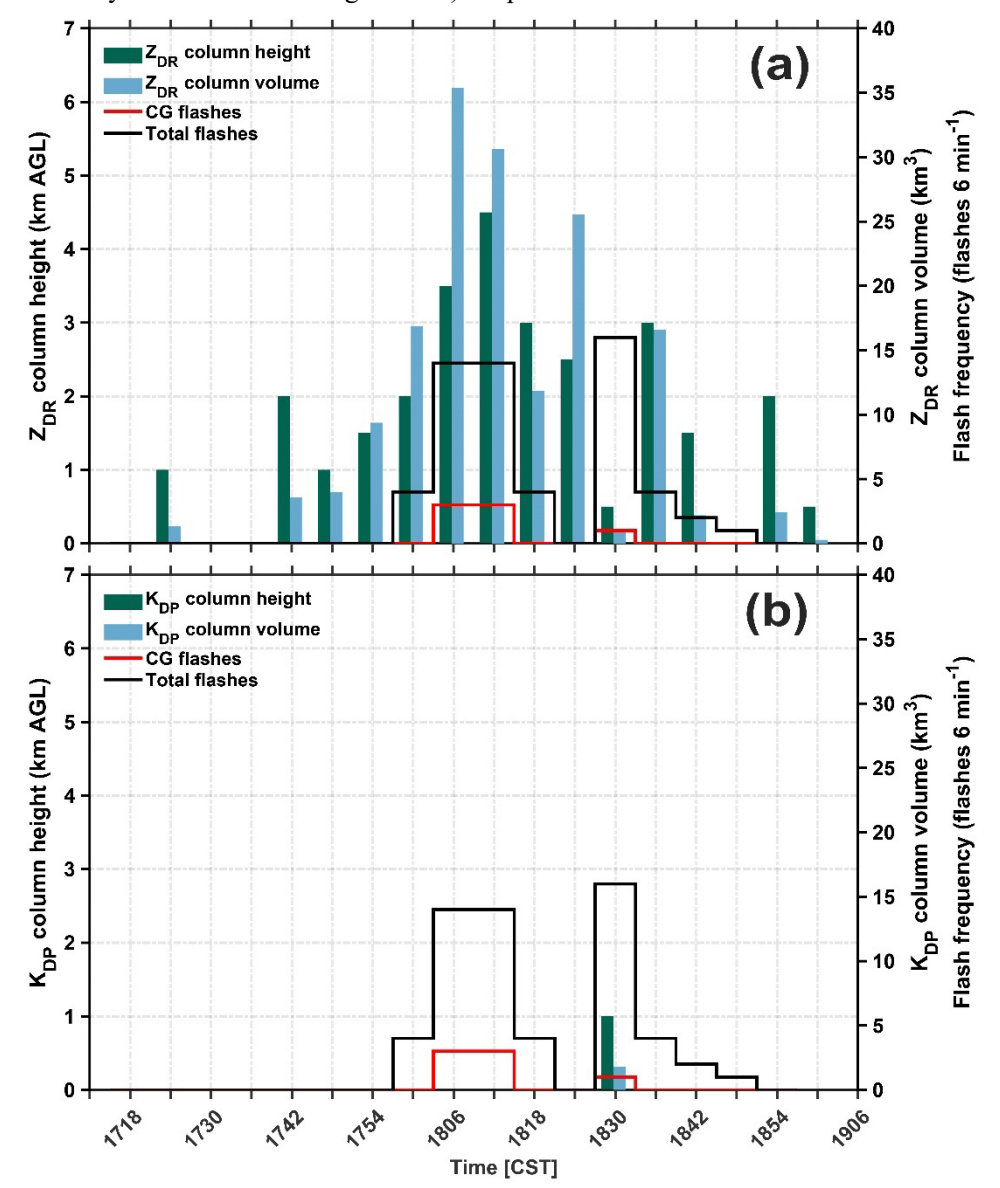


Figure 5. Time–height (volume) variation in the Z_{DR} column (a) and K_{DP} column (b). The dark green bars indicate the column heights and the light blue bars indicate the column volumes. The black (red) stepped line indicates the total flashes (CG flashes) from the LFEDA. AGL (above ground level).

Although large ice particles form and fall, the K_{DP} column is absent. However, a K_{DP} core with high values ($\geq 1^{\circ}$ /km) occurs near the location where large ice particles (approximately 50 dBZ) melt, and a shedding process may occur, resulting in a K_{DP} core (Figure 4e). At 18:30 CST, the lightning activity reaches the second peak (Figure 6), but the Z_{DR} column almost disappears;

interestingly, the K_{DP} column forms, with high values expanding downwards to the bottom of the cloud (Figure 4d, f). In addition, the K_{DP} column only occurs at 18:30 CST, which corresponds to the second peak of lightning activity (Figure 5b).

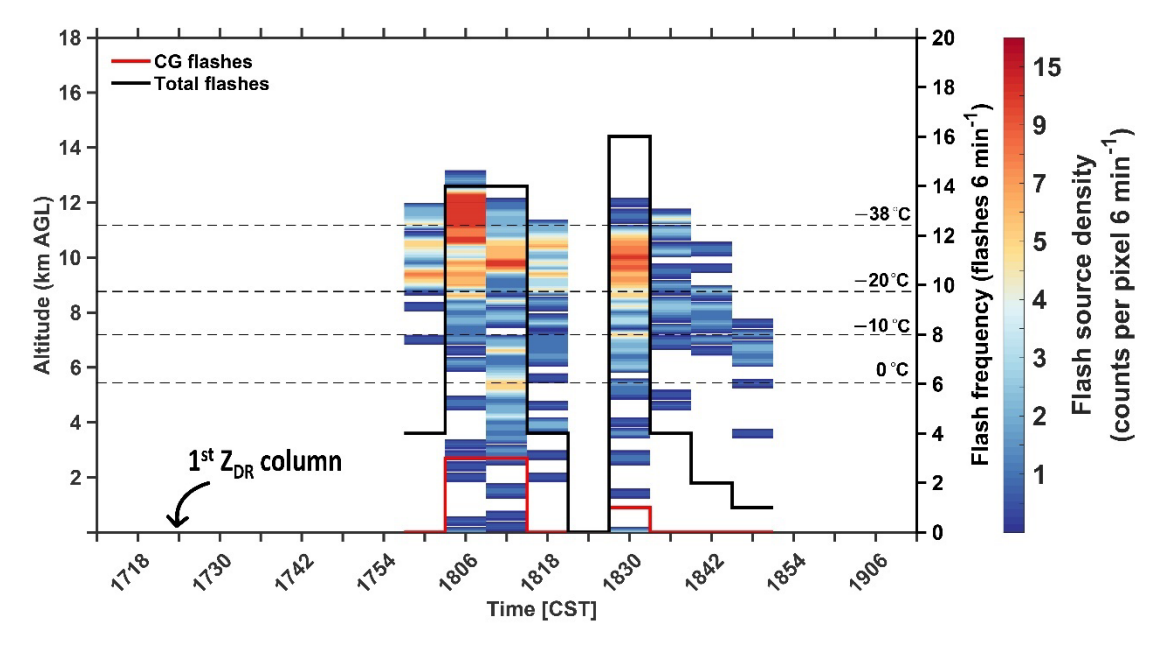


Figure 6. Time-height variation in flash source density (count per pixel, 6 min⁻¹). The black (red) stepped line indicates the total flashes (CG flashes) from the LFEDA. The dashed lines indicate the isotherm heights from 0 to -38°C. AGL (above ground level).

3.2 Vertical structures of microphysics related to lightning activity

To study the vertical thunderstorm structure related to lightning activity, we explore the vertical structures of polarimetric radar variables and microphysics, in combination with 3D lightning location data. Figure 7 displays the cross sections of polarimetric radar variables (Z_H , Z_{DR} , and K_{DP}) and microphysics (hydrometeor types and microphysical fingerprints) from the Cartesian grid of the studied isolated thunderstorm. At 18:00 CST (Figure 7 a1-e1), the lightning activity begins, and the locations of the flash sources are high and correspond mainly to graupel particles. Riming occurrence surrounds the flash sources. The Z_{DR} column and reflectivity core (\geq 40 dBZ) begin to separate, having previously been overlapping during the initial development stage of the thunderstorm (Figure 4a, b). Then, at 18:06 CST (Figure 7 a2-e2), riming begins obviously, the echoes strengthen (\geq 55 dBZ), and the heights of the strong echoes are lifted. This finding indicates that the convective strength or updrafts are obviously increased and that the cold cloud processes are heavily. The lightning activity reached the first peak, where the locations of the flash sources

mainly corresponded to graupel and ice particles. Moreover, the Z_{DR} column is located at the periphery of the reflectivity core, and high K_{DP} values occur and correspond to heavy rain particles, which are associated with large ice particles (e.g., hailstones) melting, raindrops coalescence and/or break. This phenomenon is consistent with that the K_{DP} tends to be directly proportional to the rain mixing ratio (Snyder et al., 2017).

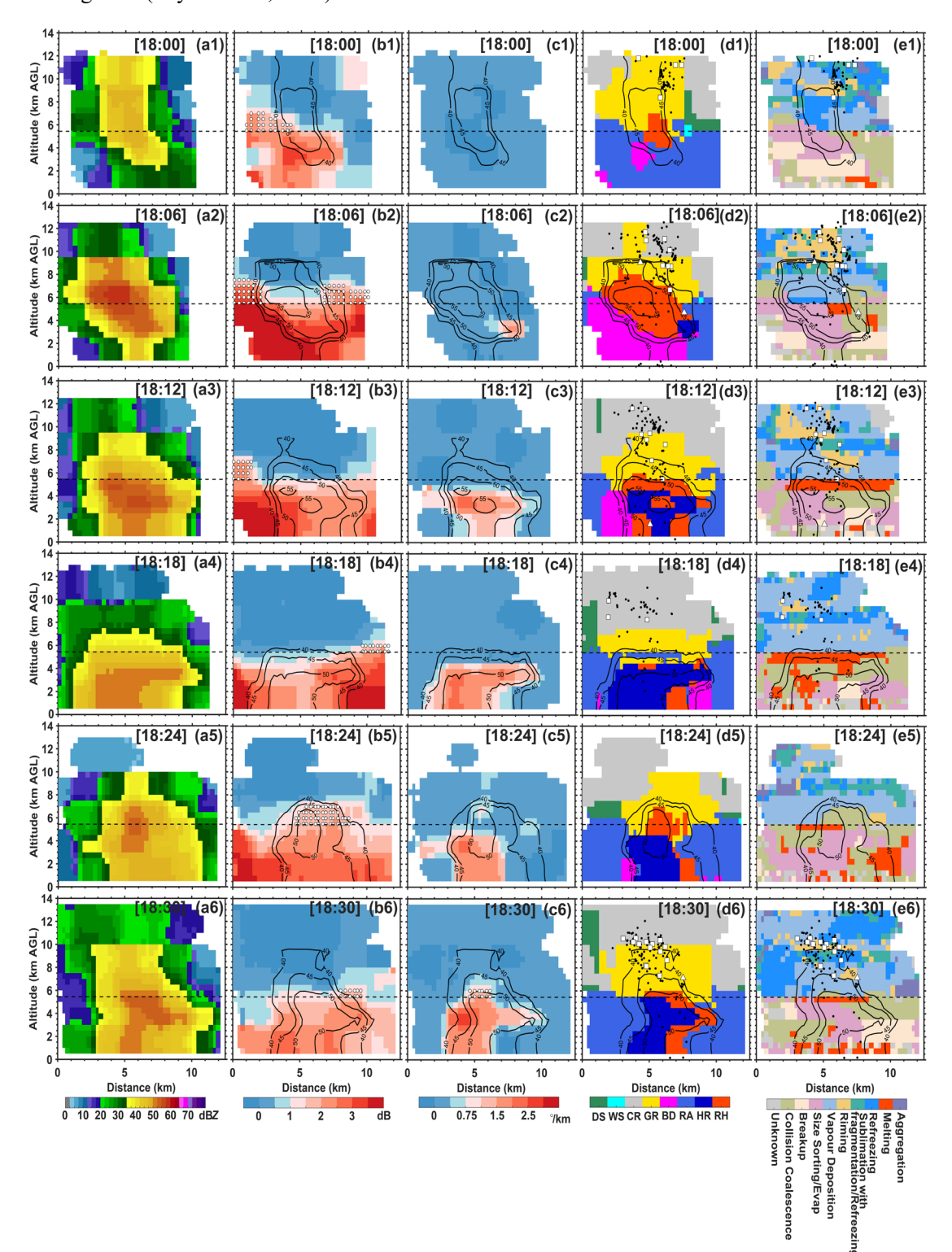


Figure 7. Cross sections of polarimetric radar variables (Z_H, Z_{DR}, and K_{DP}) and microphysics (hydrometeor types and microphysical fingerprints) from the Cartesian grid of the isolated thunderstorm (case #1). At 18:00 CST (a1-e1), 18:06 CST (a2-e2), 18:12 CST (a3-e3), 18:18 CST (a4-e4), 18:24 CST (a5-e5), and 18:30 CST (a6-e6). The black dashed line indicates the 0°C isotherm height. The white dots indicate the areas of the identified Z_{DR}/K_{DP} columns. The black contours with values indicate the reflectivity structure. The black dots indicate the flash sources, the white square represents the first source of the intracloud flash, and the triangle represents the CG

flash.

Subsequently, the lightning activity weakened at 18:12 and 18:18 CST. During this stage (Figure 7 a3-e3, a4-e4), the reflectivity core is landing and large ice particles above the melting level decrease, corresponding to heavy melting and indicating increasing downdrafts. Although Z_{DR} columns are present, they can only indicate updrafts around the reflectivity core. However, the reflectivity core was lifted again at 18:24 CST (Figure 7 a5). The contents of rain and hail mixtures and graupel clearly increased (Figure 7 d5). This indicates that the convective strength or updrafts are increased. Notably, the Z_{DR} column and reflectivity core overlap again, just as occurred during the initial development of the thunderstorm (Figure 4a, b; Figure 7 b5). Although a few high K_{DP} values occurred above the melting level, a K_{DP} column formed during the next 6 minutes (Figure 7 c5, c6). At 18:30 CST (Figure 7 a6-e6), the lightning activity reaches the second peak, and the riming process surrounds these flash sources. The Z_{DR} column within the reflectivity core quickly collapses with the occurrence of abundant graupel particles.

In total, this thunderstorm shows two impulses in vertical velocity, which correspond to two lightning activity peaks. When the first impulse event initially develops, the Z_{DR} column is obvious and overlaps with the reflectivity core; however, the region of the Z_{DR} column within the reflectivity core will collapse, with abundant graupel particles forming by riming or freezing, stimulating updrafts and intensified lightning. When large ice particles (e.g., graupel or hailstone) subsequently decrease, indicating the end of the first impulse event, melting and shedding processes occur, resulting in more raindrops (many moderate-to-large and small raindrops) contributing to high Z_{DR}/K_{DP} values. These raindrops could recirculate into the updrafts and be lifted to the mixed-phase region, forming the Z_{DR} column first, and raindrops could transfer to abundant graupel and even hailstones, releasing latent heat and thus invigorating updrafts again (indicating the second impulse

event). However, the Z_{DR} column within the reflectivity core will collapse with increasing amounts of graupel and/or hailstone particles, but the K_{DP} column will occur; this can be explained by the increased K_{DP} values at the column top being associated with an increasing number of small-to-moderate hailstones with significant water fraction (Snyder et al., 2017). The lightning activity also reaches a peak value.

Thus, the Z_{DR} column within the reflectivity core is likely an indicator of imminent convection invigoration via latent heat release and then the formation of abundant graupel particles promotes lightning activity via noninductive charging; the K_{DR} column is highly related to cold cloud processes, replacing Z_{DR} column to indicate updrafts within the reflectivity core when obvious graupels and hailstones occur.

3.3. The polarimetric and microphysical characteristics within the Z_{DR} columns

Figure 8 shows the normalized distributions of the polarimetric and microphysical characteristics within the series of Z_{DR} columns during the life cycle of the studied thunderstorm. The Z_H values within the Z_{DR} columns range from approximately 10 to 55 dBZ; specifically, weak reflectivity is present in the initial phase of the thundercloud (Figure 8a). This suggests the use of the Z_H threshold value (e.g., 25, 40, or 35–50 dBZ) to help select Z_{DR} columns results in the loss of information, especially for the initial phase of clouds. The increase in reflectivity intensity within the Z_{DR} columns can be used to predict lightning activity, and the peaks in both reflectivity intensity and lightning activity are consistent. A strong reflectivity intensity peak is associated with a high number of lightning flashes (Figure 8a).

The Z_{DR} values within the Z_{DR} columns range from approximately 1.5 to 4 dB, and the increasing trend of the Z_{DR} values is consistent with the first peak of lightning activity but has a low correlation with the second peak of lightning activity (Figure 8b). The pattern of D_0 within the Z_{DR} columns is similar to that of the Z_{DR} values, depending on the strong linear relationship between D_0 and Z_{DR} (Figure 8c). The liquid water content within the Z_{DR} columns ranges from approximately 0.1 to 4 gm⁻³, and the peaks correspond to the two peaks of lightning activity (Figure 8d).

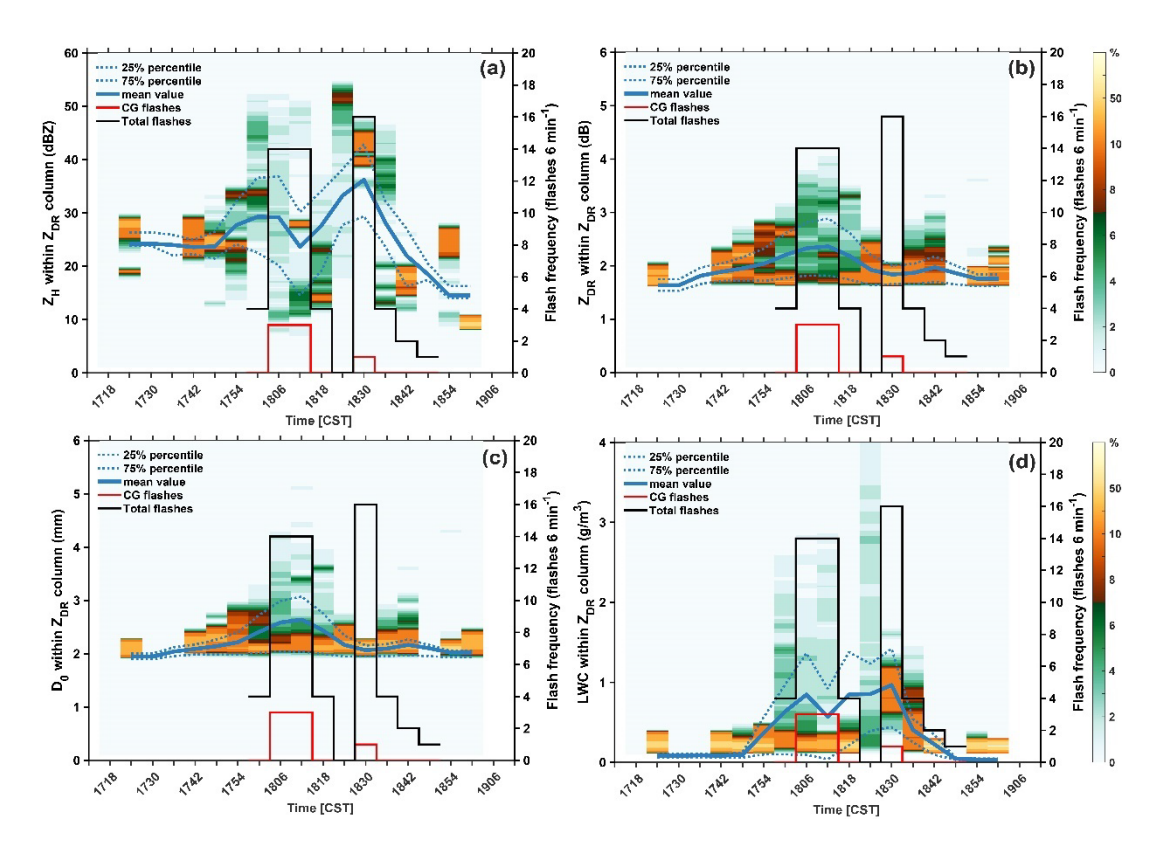


Figure 8. The normalized distributions of the polarimetric and microphysical characteristics within the series of Z_{DR} columns. (a) Z_{H} . (b) Z_{DR} . (c) Median volume diameter (D_0) of raindrops. (d) Liquid water content (LWC). The blue solid line indicates the mean value. The shading indicates the normalized occurrence frequency (unit: %). The blue dashed lines indicate the 25% and 75% percentiles. The black (red) stepped line indicates the total flashes (CG flashes) from LFEDA, and the lightning flash frequency is counted every 6 minutes.

In addition, the percentage of hydrometeors within the Z_{DR} columns is investigated on the basis of the retrieved contents of ice (including graupel) or raindrops, as described in Section 2b. The results of hydrometeor identification are dominated by large size particles. Thus, we count the grids of ice (graupel) or raindrops via the results of the Z_{DP} method to investigate the percentage of hydrometeors within the Z_{DR} columns, avoiding neglecting the grid that possesses both ice (graupel) particles and liquid drops simultaneously. The obvious phenomenon is that the percentage of graupel within the Z_{DR} columns suddenly peaks before the first peak of lightning activity, but the second peak of lightning activity is not related to the presence of graupel within the Z_{DR} columns; the hydrometeor type within the Z_{DR} column at 18:30 CST is raindrops (Figure 9). Notably, the results neglect raindrops that smaller than 1 mm; although these small raindrops are a minor within the Z_{DR} column. This indicate the collapse of the Z_{DR} column within the reflectivity core at 18:30 CST, which is consistent with the results shown in Figure 4d; the large-sized ice particles (i.e., graupel,

corresponding to the reflectivity core) fall from aloft, and the smaller Z_{DR} values of such ice particles result in this collapse phenomenon. Thus, the retained Z_{DR} column corresponds to the periphery of the reflectivity core, indicating relatively weak updrafts and raindrops. Notably, the absence of graupel within the Z_{DR} columns does not mean that the graupel particles are eliminated within the clouds. On the other hand, the sudden increase in graupel within the Z_{DR} column at 18:00 CST may support the presence of a coalescence—freezing mechanism that led to graupel formation in the warm-based clouds. The hypothesis about coalescence—freezing mechanism was proposed in previous studies (e.g., Braham, 1986; Bringi, et al., 1997; Carey and Rutledge, 2000; Herzegh and Jameson, 1992).

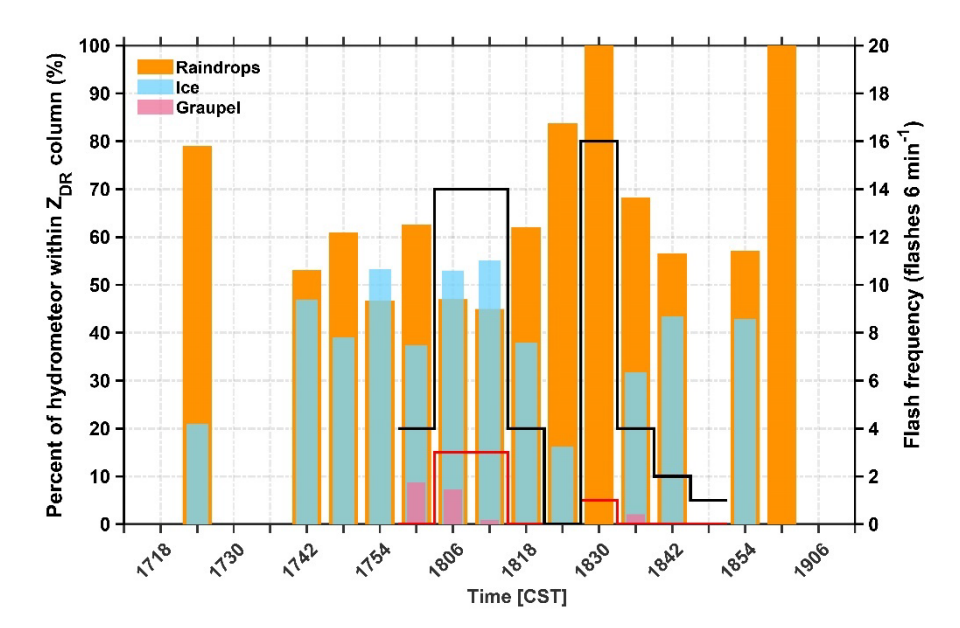


Figure 9. The percentages of hydrometeors within the series of Z_{DR} columns. The orange bars indicate the percentage of raindrops. The blue bars indicate the percentage of ice particles (including graupel). The pink bars indicate the percentage of graupel. The black (red) stepped line indicates the total flashes (CG flashes) from LFEDA, and the lightning flash frequency is counted every 6 minutes.

3.4. Statistical results

To determine the relationship between lightning activity and the quantified Z_{DR} columns, the height and volume of the Z_{DR} column are calculated via the "3D mapping column" method; the volume is based on the accumulation of all grids within the Z_{DR} column, and the volume of a single grid is 0.03125 km³, with 0.25-km horizontal and 500-m vertical resolutions. The height of the Z_{DR}

column is determined by counting the grid number (n) from the melting level to the highest grid within the Z_{DR} column; if n is determined, the Z_{DR} column height is $n \times 0.5$ km.

The variations in the Z_{DR}/K_{DP} column height and volume with the life cycle of the remaining fourteen cases are displayed in Figures 10 (cases #2 to #8) and 11 (cases #9 to #15), as are the variations in the percentages of hydrometeor types and microphysical fingerprints. The grid is assigned to specific particle type based on the results of hydrometeor identification, and the percentage of grids for each hydrometeor type is calculated. Similarly, this process is applied to determine the percentage of grids associated with microphysical fingerprints. Each of them has a Z_{DR} column (Figure 10 a1-a7, Figure 11 a1-a7); however, the absence of a K_{DP} column is possible (Figures 10 b1-b7, Figures 11 b1-b7). The results of our study support the observations of Bruning et al. (2024), namely, lightning is not observed in the absence of a Z_{DR} column, and a K_{DP} column is not observed without a Z_{DR} column. Moreover, the highest lightning flash frequency (in case #11) is observed when the Z_{DR} and K_{DP} columns are co-present, which is consistent with the observations of Bruning et al. (2024). In addition, our results suggest that the signal in the K_{DP} column within these small, isolated, subtropical thunderstorms over South China is not as steady as that in the Z_{DR} column during the life cycle.

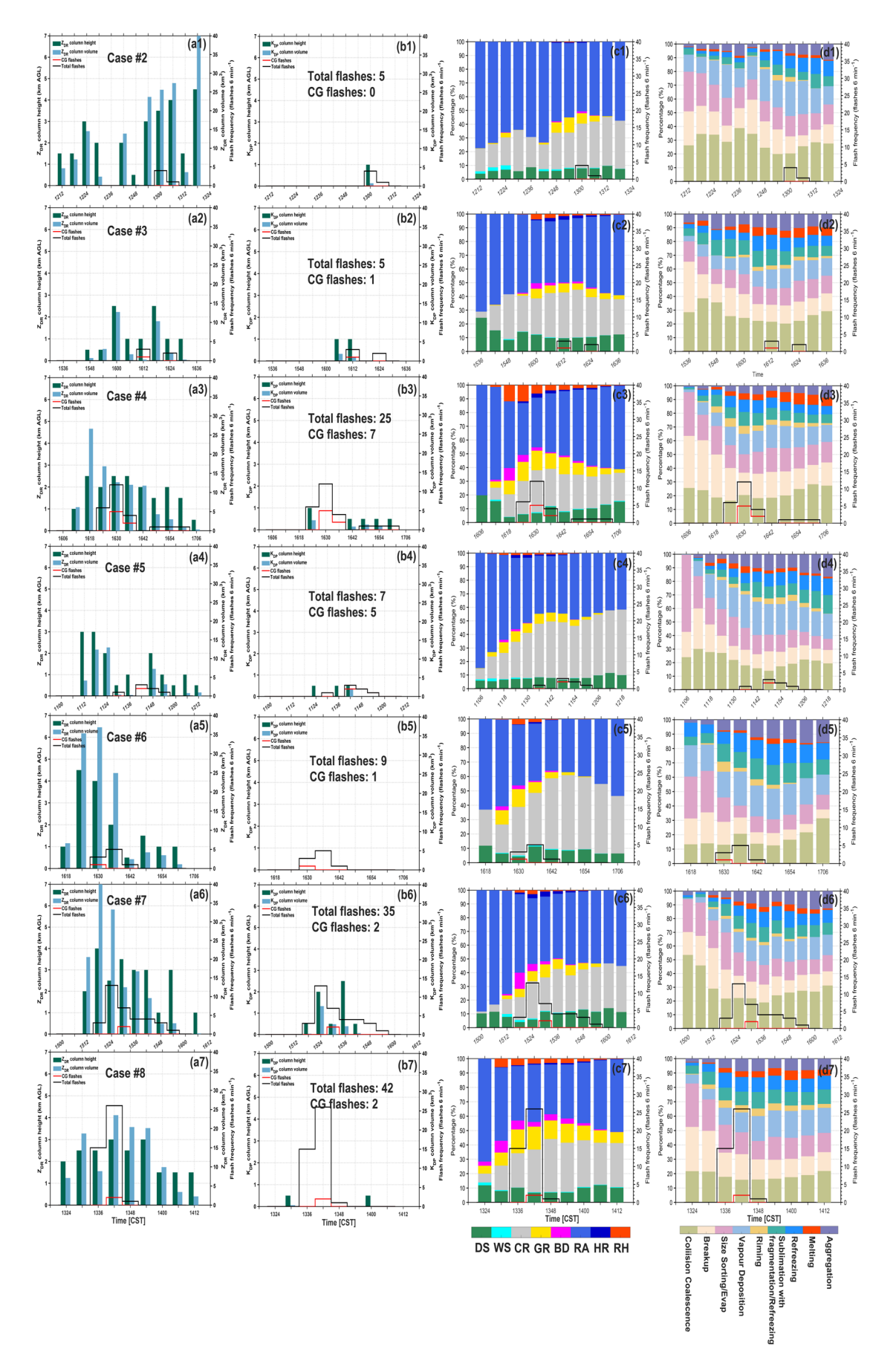


Figure 10. The variation in Z_{DR} column height and volume with the life cycle of thunderstorms (cases #2 to #8) (a1-a7). The variation in the K_{DP} column height and volume with the life cycle of thunderstorms (cases #2 to #8) (b1-b7). The dark green bars indicate the column heights, and the light blue bars indicate the column volumes. The texts display the number of total flashes and CG flashes in a thunderstorm. The variation in percentages of hydrometeor types with the life cycle of thunderstorms (cases #2 to #8) (c1-c7). The variation in percentages of microphysical fingerprints with the life cycle of thunderstorms (cases #2 to #8) (d1-d7). The black stair lines indicate the total flashes, and the red stair lines indicate the CG flashes.

The results show that the percentages of identified graupel particles and riming process are

The results show that the percentages of identified graupel particles and riming process are closely related to lightning activities (Figures 10 c1-c7, d1-d7 and Figures 11 c1-c7, d1-d7), which are consistent with that in Figure 7. The cross-correlation approach can be used to examine the correlation considering the time lag, which is important for verifying whether a parameter is appropriate for forecasting another parameter. To further determine the correlation between lightning activity and the polarimetric structure. The cross correlations between the lightning activity and polarimetric structure during the life cycles in all the cases are examined, and the results are displayed in Figure 12.

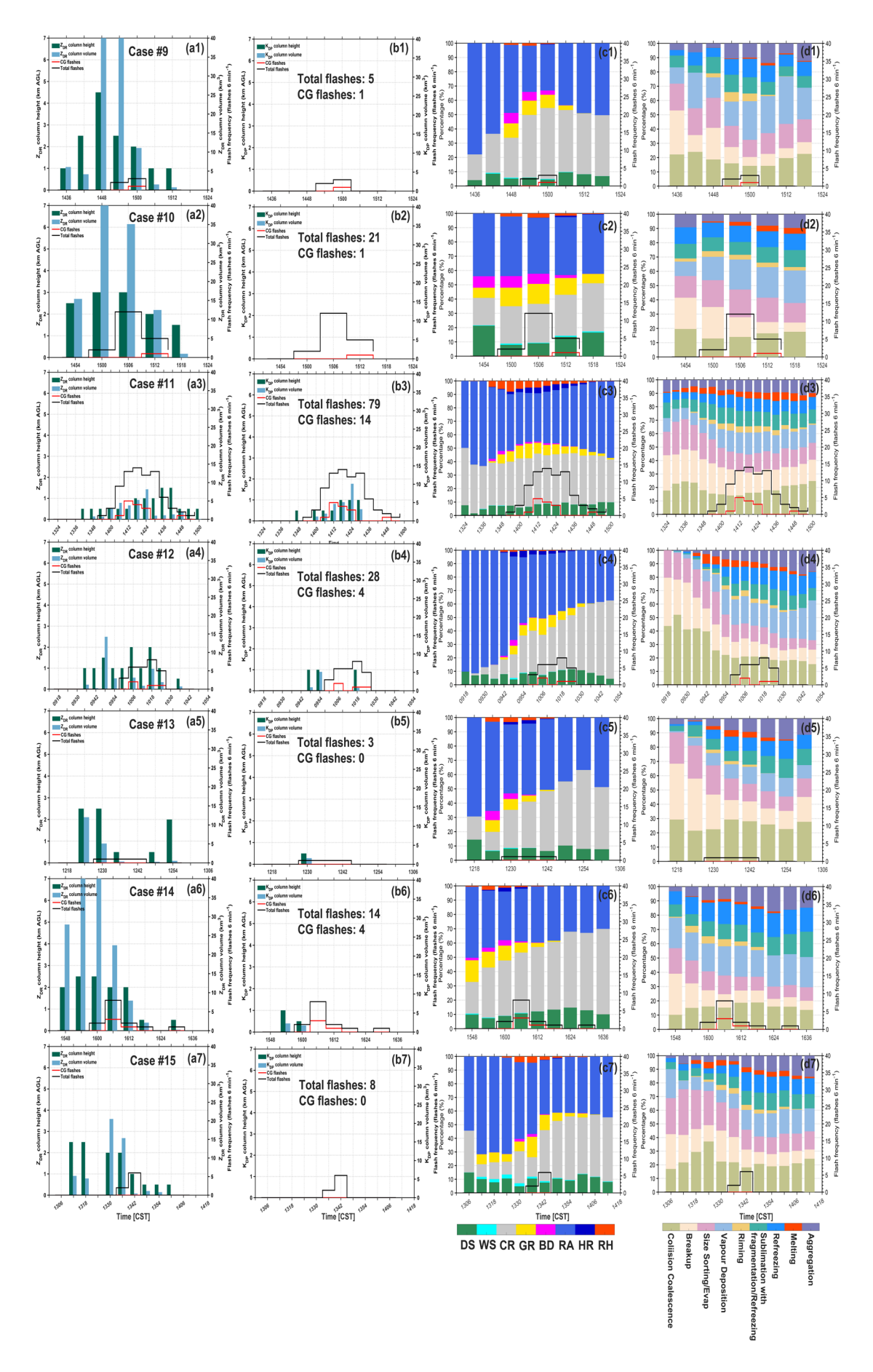


Figure 11. The variation in Z_{DR} column height and volume with the life cycle of thunderstorms (cases #9 to #15) (a1-a7). The variation in the K_{DP} column height and volume with the life cycle of thunderstorms (cases #9 to #15) (b1-b7). The dark green bars indicate the column heights, and the light blue bars indicate the column volumes. The texts display the number of total flashes and CG flashes in a thunderstorm. The variation in percentages of hydrometeor types with the life cycle of thunderstorms (cases #9 to #15) (c1-c7). The variation in percentages of microphysical fingerprints with the life cycle of thunderstorms (cases #9 to #15) (d1-d7). The black stair lines indicate the total flashes, and the red stair lines indicate the CG flashes.

Figure 12a shows that the variation in the graupel or rain water content above the melting level within the cloud can predict the lightning activity (total flashes) after 6 minutes well, and the correlation coefficient is approximately 0.8. However, other parameters (e.g., Z_{DR} column volume, ice content above the melting level, and graupel volume) also exhibit good performance in forecasting lightning activity, and the correlation coefficient can reach approximately 0.7. The graupel volume is calculated based on the identification results of hydrometeors. Although the variation in the graupel or rain water content above the melting level within the cloud can also forecast the lightning activity (CG flashes) after 6 minutes, the correlation coefficient decreases to approximately 0.56 (Figure 12b). Notably, the trend of the Z_{DR} column volume implies that it may perform well with a longer warning time (e.g., 12 minutes) for lightning activity.

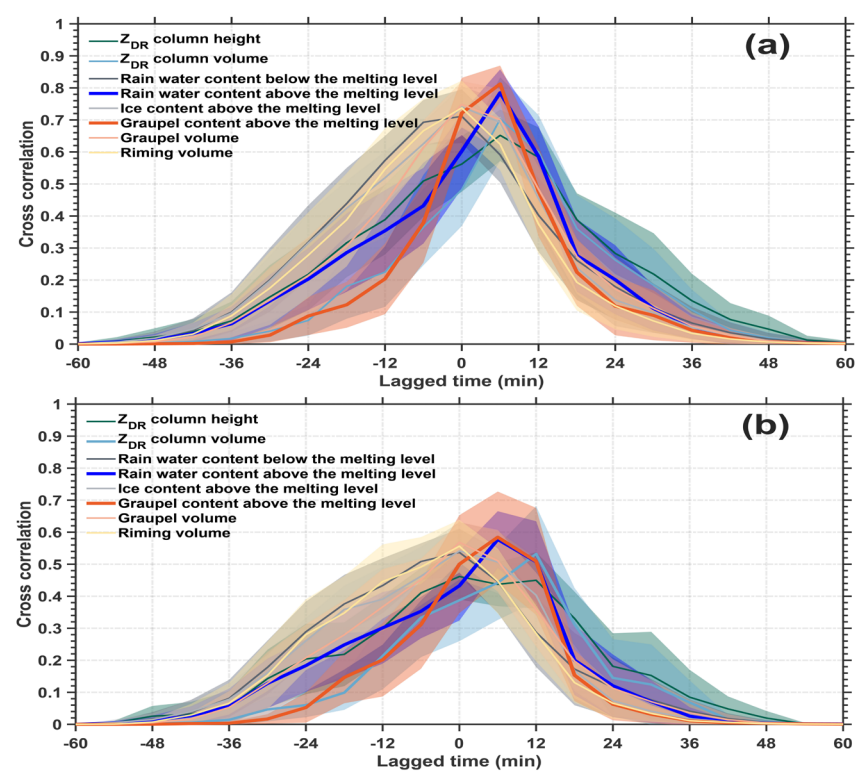


Figure 12. Cross-correlations between flash frequency (total flashes (a), CG flashes (b)) and eight radar-retrieved variables (Z_{DR} column height/volume, rain water content below/above the melting level, ice content above the melting level, graupel content above the melting level, graupel volume, and riming volume); the lines indicate the mean values and the shaded area indicates the 95% confidence interval. The lagged time is for flash frequency lags these eight radar-retrieved variables.

4. Conclusion and discussion

The relationship between the polarimetric structure and lightning activity is evaluated within fifteen isolated thunderstorm cells during the cloud life cycle in this study. We focus on the proxies of cloud updrafts and supercooled liquid raindrops (Z_{DR} or K_{DP} columns) and the content of ice or rainwater, which have been demonstrated to be related to the variations in the number of lightning flashes in previous studies (e.g., Bruning et al., 2024; Carey and Rutledge, 2000; Hayashi et al., 2021; Sharma et al., 2024; Sharma, et al., 2021; van Lier-Walqui, et al., 2016). Furthermore, we explore the microphysical fingerprints, which should be related to column formation and lightning activity. Therefore, the objective of this study is to clarify the sequence and interactions of these parameters for predicting lightning activity during the cloud life cycle and understanding the corresponding cloud microphysics.

To precisely identify and quantify the Z_{DR} or K_{DP} columns within an isolated thunderstorm during the whole cloud life cycle, the "3D mapping columns" method is improved; it is based on the morphology and high values of the Z_{DR} or K_{DP} columns in Cartesian grid data. The "3D mapping columns" method has advantages in identifying Z_{DR} columns in the initiation phase of convective clouds, avoiding the utilization threshold value of Z_{H} . The volume and height of the Z_{DR} columns are quantified via the "3D mapping columns" method, and the correlation coefficient indicates that the volume of the Z_{DR} column is better for forecasting lightning activity than the column height is. In addition, both the volume and height of a Z_{DR} column have some limitations in forecasting lightning activity, except during the early phase. This phenomenon is similar to the results of Sharma et al. (2024). In their study, the correlation coefficient between the Z_{DR} column volume and total flash rate generally monotonically decreased after the initial lightning jump, and the volume of the K_{DP} columns exhibited relatively high co-variability with the total flash rate, except in the early phase. The time lag between the formation of the Z_{DR} column and that of the Z_{DR} column was

consistent with the results of this study, indicating the different formation mechanisms of the Z_{DR} and K_{DP} columns described in Section 1.

As discussed in Section 3.2, lightning activity is indeed related to dynamic variation and impulses in vertical velocity, which is consistent with the findings of previous studies (e.g., Bruning et al., 2024; Sharma et al., 2024; Sharma et al., 2021). The unsteady Z_{DR} and K_{DP} columns are tied to unsteady updrafts associated with thermal bubbles, which are relatively short-lived and thus indicate an impulse in vertical velocity. In this way, the variations in the Z_{DR} and K_{DP} columns can indicate lightning activity. Although this hypothesis is reasonable and supported by observations through the microphysical signatures of large-drop lofting and glaciation corresponding to the Z_{DR} and K_{DP} columns (Bruning et al., 2024; Fridlind et al., 2019); however, the observations of Sharma et al. (2024) and Sharma et al. (2021) revealed that the K_{DP} column volumes (or mean K_{DP} values within a segmented K_{DP} column) have noticeably different pattern than the Z_{DR} column volumes (or mean Z_{DR} values within a segmented Z_{DR} column), which has remained a question in Sharma et al. (2021).

In this study, we explore the polarimetric and microphysical structures related to impulse events and lightning activity. The results indicate that the column within the reflectivity core is only the Z_{DR} column in which the impulse event initially develops; then, the supercooled raindrops indicated by the Z_{DR} column transfer to abundant graupel and/or hailstone particles, releasing latent heat and thus invigorating convection; accompanying the Z_{DR} column within the reflectivity core, it collapses, and lightning intensifies. Moreover, the formation of the K_{DP} column requires melting and shedding processes from large ice particles (e.g., graupel or hailstones) that produce many raindrops of moderate-to-large and small sizes, which contribute to high Z_{DR}/K_{DP} values. These raindrops can recirculate into updrafts and be lifted to the mixed-phase region, forming the Z_{DR} column first, but then, it collapses as graupel and/or hailstone particles increase. Convection and lightning are enhanced, and a K_{DP} column is formed, which is associated with an increasing number of small-to-moderate hailstones with a significant water fraction. Thus, the Z_{DR} and K_{DP} columns within the reflectivity core are associated with the different stages of an impulse event, the Z_{DR} column indicates the stage in which cold cloud processes are weak, and the K_{DP} column is the opposite of the Z_{DR} column. This may explain the remaining question in Sharma et al. (2021),

namely, why the K_{DP} column has a noticeably different pattern than the Z_{DR} column does. Notably, the Z_{DR} column is located at the periphery of the reflectivity core when the Z_{DR} column collapses within the reflectivity core.

We bridged the polarimetric structure (the Z_{DR}/K_{DP} column, supercooled liquid water, and graupel content below 0°C) and lightning activity on the basis of observations of fifteen isolated thunderstorm cells (the variation curve is conceptualized in Figure 13). The two peaks of lightning activity in Figure 13 suggest multiple impulse events in convection; specifically, the first peak refers specifically to the initial impulse event, but the second peak suggests subsequent impulse events. The magnitude of the amplitudes among these curves has no practical meaning; it is merely for visualization purposes.

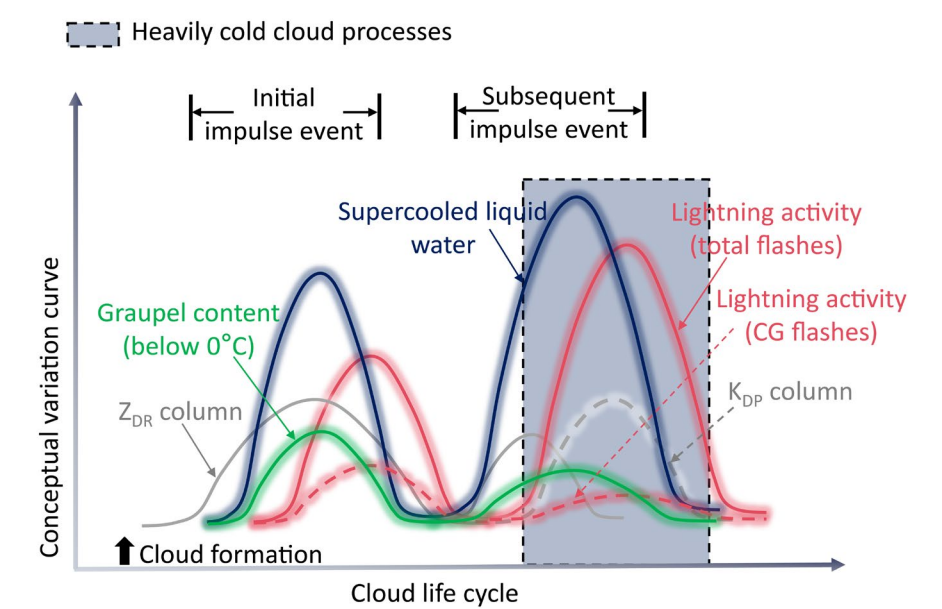


Figure 13. A conceptual model bridging the polarimetric structure and lightning activity.

In our opinion (Figure 13), the Z_{DR} column within the reflectivity core is likely an indicator of imminent convection invigoration via latent heat release, after which the formation of abundant graupel particles promotes lightning activity via noninductive charging. Therefore, microphysics (e.g., graupel content) are more directly related to lightning activity than are dynamics (e.g., the Z_{DR} column). Moreover, the observations reveal that the microphysical variations in supercooled liquid water and graupel yield better correlation coefficients for the prediction of lightning activity at short warning times (e.g., 6 minutes in this study) than do the dynamical variations in the Z_{DR} column volume. However, the trend of the Z_{DR} column volume implies that it may perform well with a

longer warning time (e.g., 12 minutes in this study) for lightning activity. The K_{DR} column is highly related to cold cloud processes. Thus, the K_{DP} column is likely absent when the impulse event initially develops; however, it will be present later with heavily cold cloud processes, replacing the Z_{DR} column to indicate updrafts within the reflectivity core when obvious graupels and hailstones are occurring. In addition, the 6-min or 12-min warning time in our results is likely due to the temporal resolution (6 minutes) of the radar data used in this study; high temporal resolution observations of phased-array radar may decrease the uncertainty.

Notably, the threshold value for identifying the Z_{DR} column (≥ 1.5 dB) in this study is different from that (≥ 1 dB) in previous studies (e.g., Sharma et al., 2024). Although this threshold value is selected according to the retrieved raindrop diameter, which should exceed 2 mm within the Z_{DR} column during the initial phase of a storm (Kumjian, et al., 2014), the results for quantifying the Z_{DR} column (i.e., height and volume) may be different from those of previous studies that used the 1 dB threshold (e.g., Sharma et al., 2024). However, this study focuses on the trend of the Z_{DR} column height or volume; thus, the differences resulting from different thresholds are relieved. The threshold value for identifying the K_{DP} column ($\geq 1^{\circ}$ /km) in this study is consistent with that used by Sharma et al. (2024). However, the different estimation methods for K_{DP} may introduce additional uncertainty, as discussed in Sharma et al. (2021).

Moreover, the height of the melting layer (0°C), which is derived from environmental soundings, is assumed to be constant for identifying and quantifying the Z_{DR} / K_{DP} column; however, the melting level is frequently elevated within updraft cores because of latent heat release, which is influenced by the strength of updrafts relative to the ambient environment. Thus, a more accurate melting level will decrease the biased estimations of the "3D mapping columns" method in this study. In addition, although our results support some observations in Bruning et al. (2024) and seem to explain the remaining question in Sharma et al. (2024) and Sharma et al. (2021), whether there are differences between such small, isolated, subtropical thunderstorms and other thunderstorm types (i.e., mesoscale convective systems, supercells, or tropical thunderstorms) should be further analysed to reduce the probability of uncertainty in our study. Finally, although the results retrieved from hydrometeor identification and microphysical fingerprint methods are reasonable and obey

- 693 theoretical cognition in this study, the potentially biased estimates may result from isothermal height 694 and the status of the hydrometeor (e.g., canting angle). 695 Acknowledgments 696 We thank Prof. Bruning and the anonymous reviewer for their professional and constructive 697 comments and suggestions. We acknowledge the Guangzhou Institute of Tropical and Marine 698 Meteorology for collecting and archiving the radar observations. And we are also acknowledge the State Key Laboratory of Severe Weather, Chinese Academy of Meteorological Sciences & 699 700 Laboratory of Lightning Physics and Protection Engineering for three-dimensional lightning
- 701 location data.

Financial support

- 703 This research has been supported by the National Natural Science Foundation of China (grant nos.
- 42175090 and 42305079), the China Postdoctoral Science Foundation (grant no. 2023M730619),
- the Natural Science Foundation of Sichuan Province (grant no. 2024NSFSC0771), and the Scientific
- 706 Research Fund of Chengdu University of Information Technology (grant nos. KYTZ202213,
- 707 KYQN202301, and KYQN202307).

708

709

702

Author contributions:

- 710 Conceptualization: CZ and YZ. Data curation: CZ, YZ, DZ, SD, and WY. Formal analysis: CZ, YZ,
- 711 XP, and YD. Funding acquisition: YZ and CZ. Investigation: CZ, YZ, and XP. Methodology: CZ,
- 712 YZ, HZ, ZL, and DZ. Project administration: YZ. Resources: CZ and YZ. Software: CZ, HZ, and
- 713 ZL. Supervision: YZ. Validation: CZ and YZ. Visualization: CZ and YZ. Writing (original draft):
- 714 CZ, YZ, and XP.

Competing interests:

716 The contact author has declared that none of the authors has any competing interests.

717

715

- 718 **Data and materials availability:** All data in this study can be obtained from an open repository
- 719 Figshare (Zhao, 2024).

720

721 References

Amiot, C. G., Carey, L. D., Roeder, W. P., McNamara, T. M. and Blakeslee, R. J.: C-band Dual-

- Polarization Radar Signatures of Wet Downbursts around Cape Canaveral, Florida. Weather and Forecasting, 34(1): 103-131, 10.1175/waf-d-18-0081.1, 2019.
- Baker, M. B., Blyth, A. M., Christian, H. J., Latham, J., Miller, K. L. and Gadian, A. M.:
- Relationships between lightning activity and various thundercloud parameters: satellite and
- 727 modelling studies. Atmospheric Research, 51: 221-236, 10.1016/S0169-8095(99)00009-5, 1999.
- Baker, M. B., Christian, H. J. and Latham, J.: A computational study of the relationships linking lightning frequency and other thundercloud parameters. Quarterly Journal of the Royal Meteorological Society, 121(527): 1525-1548, 10.1002/qj.49712152703, 1995.
- Braham, R. R. Jr.: The cloud physics of weather modification. Part 1: Scientific basis. WMO Bulletin, 35, 215–221, 1986.
- Bringi, V. N. and Chandrasekar, V.: Polarimetric Doppler Weather Radar: Principles and Applications. Cambridge University Press, Cambridge. 2001.
- Bringi, V. N., Knupp, K., Detwiler, A., Liu, L., Caylor, I. J. and Black, R. A.: Evolution of a Florida Thunderstorm during the Convection and Precipitation/Electrification Experiment: The Case of 9 August 1991. Monthly Weather Review, 125(9): 2131-2160, https://doi.org/10.1175/1520-0493(1997)125<2131:EOAFTD>2.0.CO;2, 1997.
- Bringi, V. N., Liu, L., Kennedy, P. C., Chandrasekar, V. and Rutledge, S. A.: Dual Multiparameter
 Radar Observations of Intense Convective Storms: The 24 June 1992 Case Study. Meteorology
 and Atmospheric Physics, 59: 3-31, 10.1007/BF01031999, 1996.
- Bruning, E. C. and MacGorman, D. R.: Theory and Observations of Controls on Lightning Flash
 Size Spectra. Journal of the Atmospheric Sciences, 70(12): 4012-4029, 10.1175/jas-d-12-0289.1, 2013.
- 746 Bruning, E. C., Brunner, K. N., van Lier-Walqui, M., Logan, T. and Matsui, T.: Lightning and Radar Measures of Mixed-Phase Updraft Variability in Tracked Storms during the TRACER Field 747 748 Campaign in Houston, Texas. Monthly Weather Review, 152, 2753-2769, 749 https://doi.org/10.1175/MWR-D-24-0060.1, 2024.
- Carey, L. D. and Rutledge, S. A.: A Multiparameter Radar Case Study of the Microphysical and Kinematic Evolution of a Lightning Producing Storm. Meteorology and Atmospheric Physics, 59(1): 33-64, 10.1007/BF01032000, 1996.
- Carey, L. D. and Rutledge, S. A.: The Relationship between Precipitation and Lightning in Tropical
 Island Convection: A C-Band Polarimetric Radar Study. Monthly Weather Review, 128(8):
 2687-2710, 10.1175/1520-0493(2000)128<2687:TRBPAL>2.0.CO;2, 2000.
- 756 Chang, W., Lee, W. and Liou, Y.: The kinematic and microphysical characteristics and associated 757 precipitation efficiency of subtropical convection during SoWMEX/TiMREX. Monthly 758 Weather Review, 143(1): 317–340. https://doi.org/10.1175/MWR-D-14-00081.1, 2015.
- Deierling, W. and Petersen, W. A.: Total lightning activity as an indicator of updraft characteristics.

 Journal of Geophysical Research: Atmospheres, 113(D16), 10.1029/2007jd009598, 2008.
- Deierling, W., Petersen, W. A., Latham, J., Ellis, S. and Christian, H. J.: The relationship between lightning activity and ice fluxes in thunderstorms. Journal of Geophysical Research: Atmospheres, 113(D15), 10.1029/2007jd009700, 2008.
- Fan, X. P., Zhang, Y. J., Zheng, D., Zhang, Y., Lyu, W. T., Liu, H. Y. and Xu, L. T.: A New Method of Three-Dimensional Location for Low-Frequency Electric Field Detection Array. Journal of Geophysical Research: Atmospheres, 123(16): 8792-8812, 10.1029/2017jd028249, 2018.

- 767 Fridlind, A. M., van Lier-Walqui, M., Collis, S., Giangrande, S. E., Jackson, R. C., Li, X., Matsui,
- 768 T., Orville, R., Picel, M. H., Rosenfeld, D., Ryzhkov, A., Weitz, R. and Zhang, P.: Use of
- polarimetric radar measurements to constrain simulated convective cell evolution: a pilot study
- with Lagrangian tracking. Atmospheric Measurement Techniques, 12(6): 2979-3000,
 10.5194/amt-12-2979-2019, 2019.
- Gatlin, P. N. and Goodman, S. J.: A Total Lightning Trending Algorithm to Identify Severe Thunderstorms. Journal of Atmospheric and Oceanic Technology, 27(1): 3-22,
- 774 10.1175/2009jtecha1286.1, 2010.
- 775 Green, A. W.: An Approximation for the Shapes of Large Raindrops. Journal of Applied
- 776 Meteorology and Climatology, 14: 1578-1583, https://doi.org/10.1175/1520-
- 777 0450(1975)014<1578:AAFTSO>2.0.CO;2, 1975.
- 778 Gremillion, M. S., and Orville, R. E.: Thunderstorm Characteristics of Cloud-to-Ground Lightning
- at the Kennedy Space Center, Florida: A Study of Lightning Initiation Signatures as Indicated
- 780 by the WSR-88D. Weather and Forecasting, 14: 640-649, 1999.
- 781 Goodman, S. J., Blakeslee, R., Christian, H., Koshak, W., Bailey, J., Hall, J., McCaul, E., Buechler,
- D., Darden, C., Burks, J., Bradshaw, T. and Gatlin, P.: The North Alabama Lightning Mapping
- Array: Recent severe storm observations and future prospects. Atmospheric Research, 76(1-4):
- 784 423-437, 10.1016/j.atmosres.2004.11.035, 2005.
- Hayashi, S., Umehara, A., Nagumo, N. and Ushio, T.: The relationship between lightning flash rate
- and ice-related volume derived from dual-polarization radar. Atmospheric Research, 248,
- 787 10.1016/j.atmosres.2020.105166, 2021.
- 788 Helmus, J. J. and Collis, S. M.: The Python ARM Radar Toolkit (Py-ART), a Library for Working
- with Weather Radar Data in the Python Programming Language. Journal of Open Research
- 790 Software, 4(1), 10.5334/jors.119, 2016.
- 791 Herzegh, P. H. and Jameson, A. R.: Observing Precipitation through Dual-Polarization Radar
- Measurements. Bulletin American Meteorological Society, 73(9): 1365-1376, 10.1175/1520-
- 793 0477(1992)073<1365:OPTDPR>2.0.CO;2, 1992.
- 794 Homeyer, C. R. and Kumjian, M. R.: Microphysical Characteristics of Overshooting Convection
- 795 from Polarimetric Radar Observations. Journal of the Atmospheric Sciences, 72(2): 870-891,
- 796 10.1175/jas-d-13-0388.1, 2015.
- 797 Hu, J. and Ryzhkov, A.: Climatology of the Vertical Profiles of Polarimetric Radar Variables and
- 798 Retrieved Microphysical Parameters in Continental/Tropical MCSs and Landfalling
- Hurricanes. Journal of Geophysical Research: Atmospheres, 127(5), 10.1029/2021jd035498,
- 800 2022.
- 801 Hubbert, J., Bringi, V. N., Carey, L. D. and Bolen, S.: CSU-CHILL Polarimetric Radar
- Measurements from a Severe Hail Storm in Eastern Colorado. Journal of Applied Meteorology
- and Climatology, 37(8): 749-775, 10.1175/1520-0450(1998)037<0749:CCPRMF>2.0.CO;2,
- 804 1998.
- Hubbert, J. C., Wilson, J. W., Weckwerth, T. M., Ellis, S. M., Dixon, M. and Loew, E.: S-Pol's
- 806 Polarimetric Data Reveal Detailed Storm Features (and Insect Behavior). Bulletin of the
- 807 American Meteorological Society, 99(10): 2045-2060, 10.1175/bams-d-17-0317.1, 2018.
- 808 Krause, J. and Klaus, V.: Identifying ZDR Columns in Radar Data with the Hotspot Technique.
- Weather and Forecasting, 39(3): 581-595, 10.1175/waf-d-23-0146.1, 2024.
- 810 Kumjian, M. R.: The Impact of Precipitation Physical Processes on the Polarimetric Radar Variables.

- Ph. D. Dissertation, The University of Oklahoma, Norman, OK, USA, 327p., 2012.
- Kumjian, M. R.: Principles and applications of dual-polarization weather radar. Part I: Description
- of the polarimetric radar variables. Journal of Operational Meteorology, 1(19): 226-242,
- 814 10.15191/nwajom.2013.0119, 2013a.
- Kumjian, M. R.: Principles and applications of dual-polarization weather radar. Part II: Warm- and
- cold-season applications. Journal of Operational Meteorology, 1(20): 243-264,
- 817 10.15191/nwajom.2013.0120, 2013b.
- Kumjian, M. R.: Principles and applications of dual-polarization weather radar. Part III: Artifacts.
- Journal of Operational Meteorology, 1(21): 265-274, 10.15191/nwajom.2013.0121, 2013c.
- 820 Kumjian, M. R., Khain, A. P., Benmoshe, N., Ilotoviz, E., Ryzhkov, A. V. and Phillips, V. T. J.: The
- Anatomy and Physics of ZDR Columns: Investigating a Polarimetric Radar Signature with a
- Spectral Bin Microphysical Model. Journal of Applied Meteorology and Climatology, 53(7):
- 823 1820-1843, 10.1175/jamc-d-13-0354.1, 2014.
- 824 Kumjian, M. R., Prat, O. P., Reimel, K. J., van Lier-Walqui, M. and Morrison, H. C.: Dual-
- Polarization Radar Fingerprints of Precipitation Physics: A Review. Remote Sensing, 14, 3706,
- 826 https://doi.org/10.3390/rs14153706, 2022.
- 827 Lang, T. J. and Rutledge, S. A.: A Framework for the Statistical Analysis of Large Radar and
- Lightning Datasets: Results from STEPS 2000. Monthly Weather Review, 139(8): 2536-2551,
- 829 10.1175/mwr-d-10-05000.1, 2011.
- 830 Latham, J. and Dye, J. E.: Calculations on the electrical development of a small thunderstorm.
- Journal of Geophysical Research: Atmospheres, 94(D11): 13141-13144,
- https://doi.org/10.1029/JD094iD11p13141, 1989.
- 833 Li, H., Moisseev, D., Luo, Y., Liu, L., Ruan, Z., Cui, L. and Bao, X.: Assessing specific differential
- phase (KDP)-based quantitative precipitation estimation for the record- breaking rainfall over
- Zhengzhou city on 20 July 2021. Hydrology and Earth System Sciences, 27(5): 1033-1046,
- 836 10.5194/hess-27-1033-2023, 2023.
- Li, H. Q., Wan, Q., Peng, D., Liu, X. and Xiao, H.: Multiscale analysis of a record-breaking heavy
- rainfall event in Guangdong, China. Atmospheric Research, 232: 104703.
- https://doi.org/10.1016/j.atmosres.2019.104703, 2019.
- 840 Li, H., Yin, J. and Kumjian, M.: Z Backwards Arc: Evidence of Multi-Directional Size Sorting in
- the Storm Producing 201.9 mm Hourly Rainfall. Geophysical Research Letters, 51(10):
- e2024GL109192, https://doi.org/10.1029/2024GL109192, 2024.
- 843 Liu, D., Li, F., Qie, X., Sun, Z., Wang, Y., Yuan, S., Sun, C., Zhu, K., Wei, L., Lyu, H. and Jiang, R.:
- Charge Structure and Lightning Discharge in a Thunderstorm Over the Central Tibetan Plateau.
- 845 Geophysical Research Letters, 51(16): e2024GL109602,
- 846 https://doi.org/10.1029/2024GL109602, 2024.
- Liu, Z., Zheng, D., Guo, F., Zhang, Y., Zhang, Y., Wu, C., Chen, H. and Han, S.: Lightning activity
- and its associations with cloud structures in a rainstorm dominated by warm precipitation.
- 849 Atmospheric Research, 246, 10.1016/j.atmosres.2020.105120, 2020.
- 850 Loney, M. L., Zrnić, D. S., Straka, J. M. and Ryzhkov, A. V.: Enhanced Polarimetric Radar
- 851 Signatures above the Melting Level in a Supercell Storm. Journal of Applied Meteorology,
- 852 41(12): 1179-1194, https://doi.org/10.1175/1520-0450(2002)041<1179:EPRSAT>2.0.CO;2,
- 853 2002.
- 854 López, R. E. and Aubagnac, J.-P.: The lightning activity of a hailstorm as a function of changes in

- its microphysical characteristics inferred from polarimetric radar observations. Journal of Geophysical Research: Atmospheres, 102(D14): 16799-16813, https://doi.org/10.1029/97JD00645, 1997.
- Marshall, T. C., Rust, W. D. and Stolzenburg, M.: Electrical structure and updraft speeds in thunderstorms over the southern Great Plains. Journal of Geophysical Research: Atmospheres, 100(D1): 1001-1015, https://doi.org/10.1029/94JD02607, 1995.
- Mitzeva, R. and Saunders, C. P. R.: Thunderstorm charging: calculations of the effect of ice crystal size and graupel velocity. Journal of Atmospheric and Terrestrial Physics, 52(4): 241-245, https://doi.org/10.1016/0021-9169(90)90090-A, 1990.
- Mosier, R. M., Schumacher, C., Orville, R. E. and Carey, L. D.: Radar Nowcasting of Cloud-to-Ground Lightning over Houston, Texas. Weather and Forecasting, 26(2): 199-212, https://doi.org/10.1175/2010WAF2222431.1, 2011.
- Park, H. S., Ryzhkov, A. V., Zrnić, D. S., and Kim, K.: The Hydrometeor Classification Algorithm for the Polarimetric WSR-88D: Description and Application to an MCS. Weather and Forecasting, 24: 730-748, https://doi.org/10.1175/2008WAF2222205.1, 2009.
- Pruppacher, H. R., and Klett, J. D.: Microphysics of Clouds and Precipitation. 2d ed. Kluwer Academic, 954 pp., 1997.
- Qie, X., Yu, Y., Liu, X., Guo, C., Wang, D., Watanabe, T. and Ushio, T.: Charge analysis on lightning
 discharges to the ground in Chinese inland plateau (close to Tibet). Ann. Geophys., 18(10):
 1340-1348, 10.1007/s00585-000-1340-z, 2000.
- 875 Reynolds, S. E., Brook, M. and Gourley, M. F.: THUNDERSTORM CHARGE SEPARATION.
 876 Journal of Atmospheric Sciences, 14(5): 426-436, https://doi.org/10.1175/1520877 0469(1957)014<0426:TCS>2.0.CO;2, 1957.
- Rison, W., Thomas, R. J., Krehbiel, P. R., Hamlin, T. and Harlin, J.: A GPS-based three-dimensional lightning mapping system: Initial observations in central New Mexico. Geophysical Research Letters, 26(23): 3573-3576, https://doi.org/10.1029/1999GL010856, 1999.
- Rosenfeld, D., Lohmann, U., Raga, G. B., O'Dowd, C. D., Kulmala, M., Fuzzi, S., Reissell, A. and Andreae, M. O.: Flood or Drought: How Do Aerosols Affect Precipitation? Science, 321(5894): 1309-1313, doi:10.1126/science.1160606, 2008.
- Ryzhkov, A., and Zrnić, D.: Assessment of Rainfall Measurement That Uses Specific Differential
 Phase. Journal of Applied Meteorology and Climatology, 35: 2080-2090,
 https://doi.org/10.1175/1520-0450(1996)035<2080:AORMTU>2.0.CO;2, 1996.
- 887 Saunders, C.: Charge Separation Mechanisms in Clouds. Space Science Reviews, 137(1): 335-353, 10.1007/s11214-008-9345-0, 2008.
- Seliga, T. A. and Bringi, V. N.: Potential Use of Radar Differential Reflectivity Measurements at
 Orthogonal Polarizations for Measuring Precipitation. Journal of Applied Meteorology and
 Climatology, 15(1): 69-76, https://doi.org/10.1175/15200450(1976)015<0069:PUORDR>2.0.CO;2, 1976.
- Sharma, M., Tanamachi, R. L. and Bruning, E. C.: Investigating Temporal Characteristics of Polarimetric and Electrical Signatures in Three Severe Storms: Insights from the VORTEX-Southeast Field Campaign. Monthly Weather Review, 152(7): 1511-1536, https://doi.org/10.1175/MWR-D-23-0144.1, 2024.
- 897 Sharma, M., Tanamachi, R. L., Bruning, E. C. and Calhoun, K. M.: Polarimetric and Electrical 898 Structure of the 19 May 2013 Edmond–Carney, Oklahoma, Tornadic Supercell. Monthly

- 899 Weather Review, 149(7): 2049-2078, https://doi.org/10.1175/MWR-D-20-0280.1, 2021.
- 900 Shi, D., Zheng, D., Zhang, Y., Zhang, Y., Huang, Z., Lu, W., Chen, S. and Yan, X.: Low-frequency 901 E-field Detection Array (LFEDA)—Construction and preliminary results. Science China Earth
- 902 Sciences, 60(10): 1896-1908, 10.1007/s11430-016-9093-9, 2017.
- 903 Snyder, J. C., Bluestein, H. B., Dawson II, D. T. and Jung, Y.: Simulations of Polarimetric, X-Band
- Radar Signatures in Supercells. Part I: Description of Experiment and Simulated ρhv Rings.
- 905 Journal of Applied Meteorology and Climatology, 56(7): 1977-1999, 906 https://doi.org/10.1175/JAMC-D-16-0138.1, 2017.
- 907 Snyder, J. C., Ryzhkov, A. V., Kumjian, M. R., Khain, A. P. and Picca, J.: A ZDR Column Detection 908 Algorithm to Examine Convective Storm Updrafts. Weather and Forecasting, 30(6): 1819-1844, 909 https://doi.org/10.1175/WAF-D-15-0068.1, 2015.
- Souza, J. C. S. and Bruning, E. C.: Assessment of Turbulence Intensity in Different Spots of
 Lightning Flash Propagation. Geophysical Research Letters, 48(21): e2021GL095923,
 https://doi.org/10.1029/2021GL095923, 2021.
- 913 Straka, J. M., Zrnić, D. S. and Ryzhkov, A. V.: Bulk Hydrometeor Classification and Quantification 914 Using Polarimetric Radar Data: Synthesis of Relations. Journal of Applied Meteorology and 915 Climatology, 39: 1341-1372, https://doi.org/10.1175/1520-916 0450(2000)039<1341:BHCAQU>2.0.CO;2, 2000.
- 917 Takahashi, T.: Riming Electrification as a Charge Generation Mechanism in Thunderstorms. Journal 918 of Atmospheric Sciences, 35(8): 1536-1548, https://doi.org/10.1175/1520-919 0469(1978)035<1536:REAACG>2.0.CO;2, 1978.
- Tuttle, J. D., Bringi, V. N., Orville, H. D. and Kopp, F. J.: Multiparameter Radar Study of a Microburst: Comparison with Model Results. Journal of Atmospheric Sciences, 46(5): 601-620, https://doi.org/10.1175/1520-0469(1989)046<0601:MRSOAM>2.0.CO;2, 1989.
- van Lier-Walqui, M., Fridlind, A. M., Ackerman, A. S., Collis, S., Helmus, J., MacGorman, D. R.,
 North, K., Kollias, P. and Posselt, D. J.: On Polarimetric Radar Signatures of Deep Convection
 for Model Evaluation: Columns of Specific Differential Phase Observed during MC3E.
 Monthly Weather Review, 144(2): 737-758, https://doi.org/10.1175/MWR-D-15-0100.1, 2016.
- Vincent, B. R., Carey, L. D. Schneider, D., Keeter, K., and Gonski, R.: Using WSR-88D reflectivity data for the prediction of cloud-to-ground lightning: A central North Carolina study. Nat. Wea.

929 Dig., 27: 35-44, 2003.

- Williams, E., Boldi, B., Matlin, A., Weber, M., Hodanish, S., Sharp, D., Goodman, S., Raghavan, R.
 and Buechler, D.: The behavior of total lightning activity in severe Florida thunderstorms.
- 932 Atmospheric Research, 51(3): 245-265, https://doi.org/10.1016/S0169-8095(99)00011-3, 1999.
- 934 Williams, E. R., Weber, M. E. and Orville, R. E.: The relationship between lightning type and convective state of thunderclouds. Journal of Geophysical Research: Atmospheres, 94(D11): 13213-13220, https://doi.org/10.1029/JD094iD11p13213, 1989.
- 937 Woodard, C. J., Carey, L. D., Petersen, W. A., and Roeder, W. P.: Operational utility of dual-938 polarization variables in lightning initiation forecasting, Electronic J. Operational Meteor., 13, 939 79-102, 2012.
- 940 Yan, M., Guo, C., Ge, Z.: Numerical study of cloud dynamic-electrification in an axisymmetric, 941 time-dependent cloud model. I: Theory and model. ACTA GEOPHYSICA SINICA, 39: 52-64, 942 1996a.

- 943 Yan, M., Guo, C., Ge, Z.: Numerical study of cloud dynamic-electrification in an axisymmetric,
- 944 time-dependent cloud model. II: Calculation results. ACTA GEOPHYSICA SINICA, 39: 65-
- 945 77, 1996b.
- 246 Zhang, Y., Sun, A., Yan, M., Guo, F., Qie, X., Huang, M.: Numerical modeling for effects of electric
- activity during thunderstorms upon the growth of hail particles. Chinese Journal of Geophysics,
- 948 47(1): 25-32, 2004a.
- 249 Zhang, Y., Dong, W., Zhao, Y., Zhang, G., Zhang, H., Chen, C. and Zhang, T.: Study of charge
- 950 structure and radiation characteristic of intracloud discharge in thunderstorms of Qinghai-Tibet
- 951 Plateau. Science in China Series D: Earth Sciences, 47(1): 108-114, 10.1007/BF02880986,
- 952 2004b.
- 253 Zhang, Y., Yan, M., Sun, A., Guo, F.: Thunderstorm Electricity, China Meteorology Press, Beijing,
- 954 384 pp., 2009.
- 955 Zhao, C.: Data for "Bridging the polarimetric structure and lightning activity of isolated
- 956 thunderstorm cells during the cloud life cycle". Figshare. [Dataset].
- 957 https://doi.org/10.6084/m9.figshare.28070105.v2, 2024.
- 258 Zhao, C., Zhang, Y., Zheng, D., Li, H., Du, S., Peng, X., Liu, X., Zhao, P., Zheng, J. and Shi, J.:
- Technical note: On the ice microphysics of isolated thunderstorms and non-thunderstorms in
- 960 southern China a radar polarimetric perspective. Atmospheric Chemistry and Physics, 24(20):
- 961 11637-11651, 10.5194/acp-24-11637-2024, 2024.
- 262 Zhao, C., Zhang, Y., Zheng, D., Liu, X., Zhang, Y., Fan, X., Yao, W. and Zhang, W.: Using
- 963 Polarimetric Radar Observations to Characterize First Echoes of Thunderstorms and
- Nonthunderstorms: A Comparative Study. Journal of Geophysical Research: Atmospheres,
- 965 127(23): e2022JD036671, https://doi.org/10.1029/2022JD036671, 2022.
- 266 Zhao, C., Zhang, Y., Zheng, D., Zhou, Y., Xiao, H. and Zhang, X.: An improved hydrometeor
- 967 identification method for X-band dual-polarization radar and its application for one summer
- 968 Hailstorm over Northern China. Atmospheric Research, 245: 105075,
- 969 https://doi.org/10.1016/j.atmosres.2020.105075, 2020.
- 970 Zhao, C., Zheng, D., Zhang, Y., Liu, X., Zhang, Y., Yao, W. and Zhang, W.: Turbulence
- 971 Characteristics of Thunderstorms Before the First Flash in Comparison to Non-Thunderstorms.
- 972 Geophysical Research Letters, 48(18): e2021GL094821,
- 973 https://doi.org/10.1029/2021GL094821, 2021a.
- 274 Zhao, C., Zheng, D., Zhang, Y. J., Liu, X., Zhang, Y., Yao, W., and Zhang, W.: Characteristics of
- 975 cloud microphysics at positions with flash initiations and channels in convection and stratiform
- 976 areas of two squall lines, Journal of Tropical Meteorology, 37: 358-369,
- 977 doi:10.16032/j.issn.1004-4965.2021.035, 2021b.
- 278 Zheng, D. and Zhang, Y.: New Insights Into the Correlation Between Lightning Flash Rate and Size
- 979 in Thunderstorms. Geophysical Research Letters, 48(24): e2021GL096085,
- 980 https://doi.org/10.1029/2021GL096085, 2021.

986

- 981 Zrnić, D. S.: Complete Polarimetric and Doppler Measurements with a Single Receiver Radar.
- Journal of Atmospheric and Oceanic Technology, 8: 159-165, https://doi.org/10.1175/1520-
- 983 0426(1991)008<0159:CPADMW>2.0.CO;2, 1991.
- 984 Zrnić, D. S.: Three-body scattering produces precipitation signature of special diagnostic value.
- 985 Radio Science, 22(1): 76-86, https://doi.org/10.1029/RS022i001p00076, 1987.